Exploring regional coastal sediment pathways using a coupled tide-wave-sediment dynamics model

Davies, Alan G.; Robins, Peter; Austin, Martin; Walker-Springett, Guy

Continental Shelf Research

DOI:
10.1016/j.csr.2022.104903

Published: 15/01/2023

Peer reviewed version

Exploring regional coastal sediment pathways using a coupled tide-wave-sediment dynamics model

A.G. Davies[a,*], P.E. Robins[a], M. Austin[b], G. Walker-Springett[b]

[a] Centre for Applied Marine Sciences, School of Ocean Sciences, Bangor University, Menai Bridge, Anglesey LL59 5AB, U.K.

[b] School of Ocean Sciences, Bangor University, Menai Bridge, Anglesey LL59 5AB, U.K.

[*] Corresponding author: Email: a.g.davies@bangor.ac.uk; Tel +44 (0)1248 383933

Abstract

Knowledge of sediment transport pathways is important for coastal management as well as for offshore infrastructure such as wind farms and other renewable energy installations. Here a three-way coupled model of tides, waves and sediment dynamics is presented, which extends the approach of Davies and Robins (2017) for the prediction of the locally-varying seabed roughness k_s resulting from the interaction between the flow (tides and waves) and the bed sediment (grain size mixture) subject to wave-current interaction (WCI) at the seabed. The model was applied to the North Wales coastal area, with particular emphasis on an extensive shore-connected sand bank (Constable Bank), the stability of which was investigated through the study of residual sediment circulation patterns. Multi-beam (MBES) and seabed rig (AWAC) observations have allowed validation of the predicted k_s and hydrodynamics, respectively. With due allowance for the supply of mobile sediment, the agreement between predicted k_s and observed bedform height was generally good. The model has been used to determine residual velocities and sediment pathways, both with and without wave effects included. Wave influence and WCI are predominant in nearshore areas, affecting the magnitude and direction of the residual fluxes. A key modelling outcome offshore is a clockwise residual circulation pattern for water and sediment around the end of Constable Bank, set within a generally eastward net drift of sediment in the wider study area.

Keywords: Variable seabed roughness; Wave-current interaction; Bed friction; Residual flow; Net sediment transport; North Wales coastal area.

1. Introduction

Knowledge of sediment transport pathways in coastal areas is often limited to inferences of transport direction made from bed form asymmetry, together with some flow measurements on site. This paucity of information can give rise to uncertainties for coastal management and the design of coastal/offshore infrastructure, including wind farms and other renewable energy installations. While the relative importance of tides and waves in determining sediment transport outcomes, from deeper offshore waters to shallower coastal areas, may be understood qualitatively, it can nowadays benefit additionally from transport estimates over an entire study area made by high-resolution numerical modelling. Such an assessment of sediment movement and the resulting transport pathways is attempted here for a coastal area of great significance for future offshore renewable energy (ORE) development.

The North Wales coastal area is a highly dynamic region, subject to some of the largest tidal ranges on Earth, up to 8.5 m (Plater and Grenville, 2010), exposed to waves generated in the Irish Sea, of significant height exceeding 5 m, and also to surges of up to 2.5 m (Brown et al., 2010; Wolf et al., 2011), which can give rise to significant sediment movement. The area occupies the southern portion of greater Liverpool Bay, which has been well studied in relation to tides, waves, and freshwater input from several large English and Welsh rivers (e.g., Polton et al, 2011; Palmer and Polton, 2011; Brown et al., 2016). The complex dynamics in Liverpool Bay control the fate of freshwater input, biogeochemical pathways, coastal flooding, coastal ecosystems, sediment transport and the stability of the shoreline against a background of sea-level rise and changing weather patterns (Pope et al., 2021). These processes impact upon economically important cities such as Liverpool, because of its dredged shipping trade routes, and also upon national transport links (rail, road) that lie directly along the shore of North Wales. Further, these nearshore dynamics

are important for fisheries, aquaculture and, increasingly, the marine energy industry which hosts offshore oil and gas platforms as well as a rapidly growing wind farm sector. Potential tidal barrier installations have been investigated for estuaries such as the Mersey on the English coastline, while tidal impoundments are under consideration, as a means of both energy supply and shoreline protection, along the North Wales coast. An understanding of the sediment transport pathways throughout Liverpool Bay is, therefore, critically important for the management of the English and Welsh coastlines as well as for existing and future ORE developments.

In this paper a TELEMAC model that simulates tides, waves and sediment dynamics has been developed for the North Wales coastal area. The aim has been to assess the present-day hydrodynamic and sedimentological regimes, and sediment transport pathways in the study area, in order to assess: i) whether there is an overall west-to-east residual transport of sediment across Liverpool Bay towards the English coast, as expected from previous studies; ii) how residual transport pathways are influenced by local topographic features such as Constable Bank, a shore-connected sand bank in the centre of the domain the stability of which has great importance for future ORE developments; and iii) whether the transport pathways are tidally-dominated, due to the large tidal range present, or are influenced significantly by wave effects, particularly in shallow coastal areas. The modelling methodology used has general applicability in coastal shelf-sea areas, whether tides or waves are predominant.

The modelling approach involves a 3-way-coupling between tides, waves and sediment dynamics, extending the coupled-scheme developed by Davies and Robins (2017) through the addition of waves. The model is barotropic and two-dimensional, i.e., depth-averaged, and it has been validated using tide gauge, multibeam (MBES), and also hydrodynamic data. A key feature of the model involves the prediction of the temporally- and spatially-varying roughness (k_s) resulting from the local interaction between the flow (tides and waves) and the bed sediment (grain size mixture).

Validation of this aspect has been carried out by comparing MBES observations with the implemented k_s-predictor of Van Rijn (2007), subject to consideration of sediment supply in the study area and of the effects of waves on k_s close to shore. A new feature of the coupled model is wave-current interaction (WCI) at the seabed, which has the effect of constraining the magnitude of potentially unrealistic wave-generated currents and eddy structures near the coast. Residual velocity and sediment transport predictions provide the main modelling results.

The paper is organized as follows:- In Section 2, oceanographic and sedimentological considerations are introduced for the North Wales coastal area. The TELEMAC model setup is introduced in Section 3 and here the procedure used to model the temporally/spatially variable k_s is explained. In Section 4 the model outcomes are presented, for tides both with and without waves superimposed, focusing on residual water and sediment fluxes during a defined period of one month (May 2018). These outcomes are compared with MBES observations and other data from a rig located on Constable Bank. In Section 5 the role of wave-current interaction at the seabed and the limitations on the modelling are discussed. The conclusions of the study are presented in Section 6.

2. Liverpool Bay and the North Wales coastal domain

2.1 Oceanographic and sedimentological context

The North Wales coastal domain shown in Figure 1 is typical of many coastal regions worldwide that include sand banks, maintained channels and areas of restricted sand supply, presenting a modelling challenge not least where the seabed roughness is concerned. Sands with localised pockets of gravel and/or mud occur throughout Liverpool Bay (Pye and Blott, 2010), with large areas off the North Wales coast comprising slightly gravelly sand, though with much local variation (Plater and Grenville,2010). A general eastward directed transport residual has been inferred throughout the southern part of Liverpool Bay (Sly, 1966), resulting in movement of sediment into the Dee and other

estuaries (Pye and Blott, 2010). Plater and Grenville (2010) attributed this eastward drift to asymmetry in the tidal current ellipse, consistent with by observations of bedform asymmetry.

The sediment transport patterns are influenced primarily by strong tidal currents associated with the M_2 tide supplemented, through non-linear effects and also tidal friction, by the M_4 tidal harmonic at twice the fundamental (M_2) frequency. The S_2 tidal constituent then gives rise to spring-neap tidal modulation. The M_2 and M_4 tides combine to give a stronger flood and a weaker ebb flow of longer duration, into and out of Liverpool Bay, respectively (Horillo-Carballo et al., 2021), with the flood flow being 1.2 times faster than the ebb flow (Brown et al., 2016). These tidal currents, which are of strength up to 1 m/s in the eastern Irish Sea, weaken towards the shorelines where shoaling waves become the predominant influence on sediment transport.

Pingree and Griffiths (1979) modelled the M_2 and M_4 tidal effects and predicted that, off the entire North Wales coast, the mean, and also maximum, bottom stresses were from west to east into Liverpool Bay, in agreement with inferences of sand transport paths made earlier by Stride (1963) (also Belderson et al., 1977). Davies and Jones (1996) used a three-dimensional model to examine these frictional effects predicting a fairly-uniform pattern of near-surface residuals in the eastward direction off the North Wales coast. A similar pattern was found for the near-bed residuals which, though of smaller magnitude, were considered sufficient to potentially affect the long-term residual transport of sand. As detailed later, both baroclinic effects resulting from freshwater riverine runoff (Section 2.2), and also wave effects (Section 2.3), further influence the tidal currents and sediment transport processes throughout greater Liverpool Bay.

While previous research has been in broad agreement about the residual sediment transport being directed eastward off the North Wales coast, little detail has been published about variations in flow and transport locally, both close to the shoreline and also around salient offshore features such as

Constable Bank (Figure 1). This bank is generally considered to have been formed into a sand ridge by deposition of marine sediments since the end of the last Ice Age (Reynolds International, 2019) and, from seismic profiling, to probably be of tidal origin (Kenyon and Cooper, 2005). The bank is over 20 km long, up to 2 km wide in its outer part, and is up to 10 m high.

Kenyon and Cooper (2005) surveyed a 15 km length of the outermost part of Constable Bank. On its north side they noted a zone of active dunes (referred to as small sand waves), of wavelength mainly between 7 and 10 m, migrating to the east. Larger, regular, sharp-crested, sand waves of wavelength of about 120 m were found to cover the steeper southern side of the bank. All the sand waves, both large and small, were asymmetric in profile and steeper to the east, suggesting that net bedload transport was towards the east on both sides of Constable Bank (an inference at odds with the modelling outcomes reported in this paper). Kenyon and Cooper (2005) noted that the occurrence of the same direction of bedload on both sides of a tidal sand bank is very unusual and suggested that, if this pattern was maintained, then the bank would probably not survive for more than a few hundred years. In the deeper water, further to the south of Constable Bank, the large sand waves terminated, their crests extending only 200-300 m southwards, giving way to dunes of smaller scale.

Along the North Wales shoreline itself, sediment movement has been inferred from west to east through sediment mapping, for example as part of the Shoreline Management Plan SMP2 (Halcrow, 2011). Halcrow (2011) considered that this eastward net transport should be sufficient to balance projected future sea level rise, which is an important consideration for coastal management and the planning of future ORE developments. However, factors like increased storminess, the rate of response of coastal processes to changes in forcing conditions, and the sufficiency of sediment supply to cope with these changes, all add much uncertainty, compounded by the lack of existing

knowledge of the relationship between nearshore transport processes and the long-term transport processes offshore, including in the region of Constable Bank.

2.2 Baroclinic effects

Several previous studies of the factors influencing long-term sediment transport in the eastern part of Liverpool Bay have focussed on the density-driven circulation resulting from freshwater riverine runoff (Polton et al., 2011; Palmer and Polton, 2011; Hopkins and Polton, 2012; Bolaños et al., 2013; Brown et al., 2015, 2016). Freshwater influence arises primarily from the Dee and Mersey Estuaries and can extend westward along the North Wales coast to include much, or all, of the region of interest in this paper. Since the present model makes the assumptions of depth-averaged and barotropic flow, it is important to note at the outset the role and magnitude of baroclinic effects.

Baroclinicity involves tidal straining of the currents caused by vertical shearing. It is further subject to spring-neap tidal cyclicity, which favours stratification during the neaps and mixing on the higher, faster spring tides, modulated by seasonal cycles in heating/cooling and by the amount freshwater runoff. The process of periodic stratification yields a time varying, asymmetrical, modification to the tidal currents, subject also to wind influence (Verspecht et al., 2009).

Taken overall, the previous literature (summarised in Section 5) suggests that baroclinic effects in Liverpool Bay give rise to southward residual currents at the seabed of the order of 2 to 3 cm/s north of Constable Bank, decreasing to smaller values (probably ~1 cm/s) on its southern side and in the region of the bank itself. The magnitude of these effects is compared later with the residual currents of somewhat larger magnitude determined from the present barotropic TELEMAC simulations.

2.3 Wave effects

Waves affect the dynamics of Liverpool Bay due to local mixing within the water column and they are important for sediment resuspension in shallow water (Polton et al., 2011). The long-shore drift due to waves is also a key determining factor for net coastal sediment transport. The waves in Liverpool Bay are mainly fetch-limited with the largest fetch (~200 km) lying to the west-north-west, and with the largest waves in Liverpool Bay coming from the west through to the north. The Irish Sea is subject to severe winter storms with waves recorded since 2002 in Liverpool Bay having a largest significant wave height (H_s) of 5.4 m, with corresponding peak period (T_p) of 12 s; here H_s was less than 2 m for 93% and less than 1 m for 68% of the time (Wolf et al., 2011). The waves in Liverpool Bay are mainly generated locally within the eastern Irish Sea with long period swell largely absent and with H_s and T_p normally much less than largest values quoted above. Plater and Grenville (2010) quoted 1-in-1 year H_s and T_p values of 4.7 m and 6.8 s based on a hindcast model calibrated against wave buoy data off the North Wales coast.

3. TELEMAC model and its validation

3.1 Model domain

The present North Wales model domain shown in Figure 1 extends from the centre of the Irish Sea in the west to the English coast in the east. The sources of the bathymetric data used to construct the model grid included LiDAR data available at 2 m resolution for intertidal regions (https://lle.gov.wales/), MBES data collected by Bangor University at <5 m resolution covering various coastal regions (https://www.imardis.org/), and Admiralty chart data for deeper offshore regions (https://digimap.edina.ac.uk/).

The unstructured finite-element model grid was created using BlueKenue™ (Canadian Hydraulics Centre, 2011). It comprises 161,799 nodes, with seabed depth in the range: −157 to 20 m (referenced to Mean Sea Level, MSL). The grid size is variable, ranging from ~2 km in the outer offshore region to 25 m in the coastal zone. The locations of the Irish Weather Buoy M2 (Marine

Institute, 2020) used for definition of the wave field, and also of the tide gauges used for model validation, are shown in Figure 1. The AWAC deployed on Constable Bank provided further hydrodynamic information for model validation.

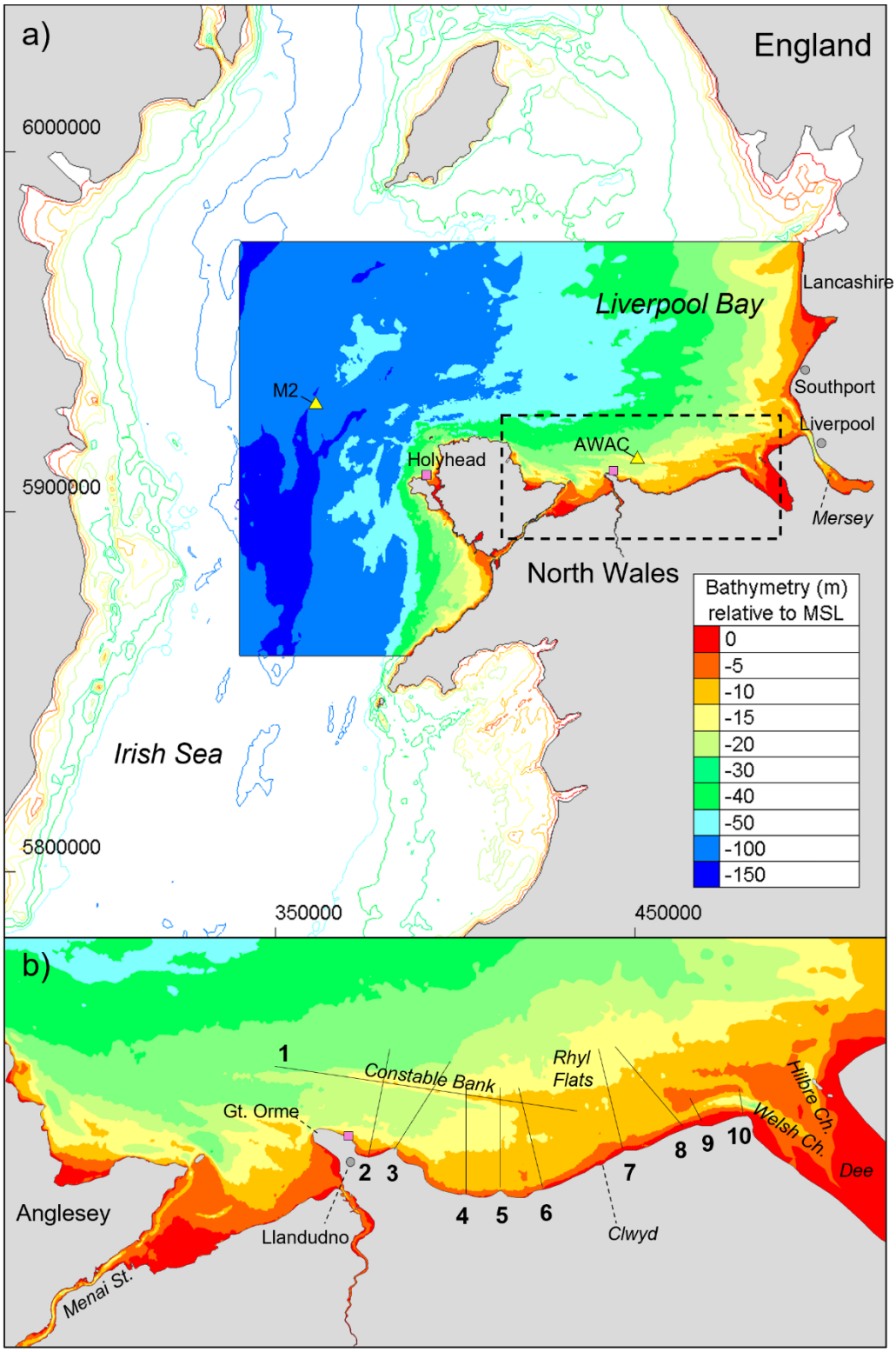

Fig. 1. (a) The model domain and bathymetry for greater Liverpool Bay and parts of the eastern Irish Sea, set within a bathymetric map of the Irish Sea. The locations of the M2 buoy and AWAC Frame 1 (triangles) and of the tide gauges (squares) are also shown. The dashed box in (a) is shown in (b): Bathymetry of the study area off the North Wales coast. Transects 1-10 were used for bed roughness validation (1: Constable Bank; 2: Llandudno; 3: Orme; 4: Colwyn Bay; 5: Llanddulas; 6: Pensarn; 7: Splash; 8: Barkby, 9: Talacre 1; 10: Talacre 2).

3.2 TELEMAC model

The TELEMAC hydro-informatic system has been presented by Hervouet (2007) and relevant aspects of its use have been described by Villaret et al. (2013). TELEMAC model v7p3r1 has been implemented for this study on Supercomputing Wales (https://www.supercomputing.wales/) using the modelling approach schematized in Figure 2; here the 3-way coupling between the computational modules is highlighted in blue, with parallel-processing implemented.

The modelling presented is for a 30-day validation period (01-30 May 2018) for which tide gauge data were available, together with extensive MBES observations used for validation of the predicted bed roughness. Further observations were made with an AWAC rig located on Constable Bank. The analysis of the model simulations is largely focussed on 28-day averages of velocity and sediment transport over two complete spring-neap cycles within the 30-day period.

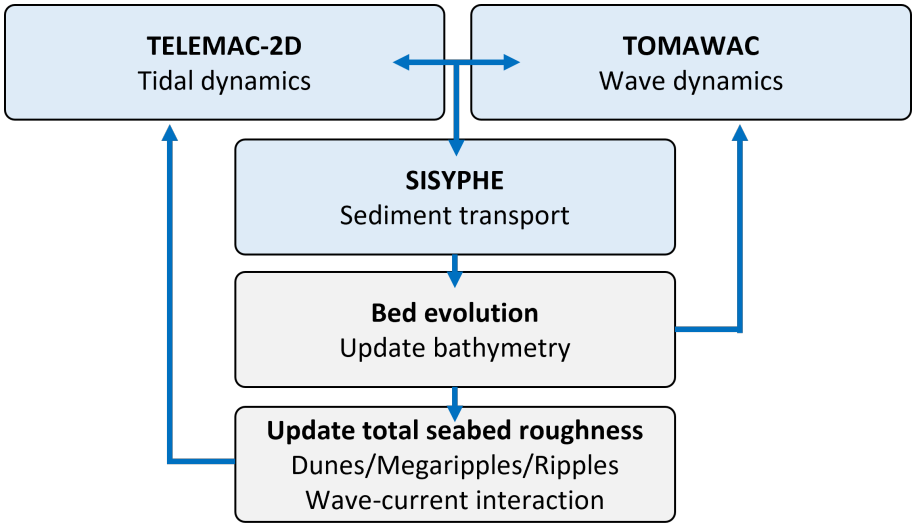

Fig. 2. Schematization of the TELEMAC model structure.

The barotropic, depth-averaged, flow module *telemac2d* was implemented here; the consequences of its neglect of baroclinic processes, referred to in Section 2.2, are assessed in Section 5. The tidal time step in *telemac2d* was 5 s, and the model output was stored every 30 min. The coupling period with wave module *tomawac* was set as 5 (i.e., coupling every 25 s) and with the sediment transport / morphology module *sisyphe* as 20 (i.e., coupling every 100 s). After each call to *sisyphe*, the bed elevation was updated, as was the locally predicted seabed roughness (k_s). A new feature of the coupled model is wave-current interaction (WCI) at the seabed. This was introduced using Soulsby and Clarke's (2005) method and, as explained in Section 5, it has the effect of constraining the magnitude of wave-generated currents.

The bed sediment was represented as a layered structure comprising a mixture of three grain diameters derived from observations by Bangor University (Unsworth et al., 2022), and the evolving k_s was predicted from the local tidal velocity, waves and sediment size using the empirical method of Van Rijn (2007) (see Appendix A). The total k_s arising from the physical roughness (dunes, mega-ripples, small-scale ripples and sediment grains), enhanced by WCI, was fed back into *telemac2d* as a part of the 3-way interaction (Figure 2).

3.3 Tidal input and validation

The tidal input used in *telemac2d* was obtained from a Princeton Ocean Model (POM) of the full shelf sea area out to the continental shelf edge (Robins et al., 2013). These results were interpolated at each of the open sea boundary points to provide values of tidal amplitude and phase at each model time step for the 5 dominant tidal constituents: M_2, S_2, N_2, K_1 and O_1. Large differences in tidal range arise at different locations in the Irish Sea; the tidal range is smallest (0.7 – 2.5 m) at the south-west corner of the domain, and largest on the Lancashire coast (3.3 – 8.7 m).

The validation sequence for May 2018 shown in Figures 3(a) and 3(b) relates to tide gauges at Holyhead and Llandudno (locations in Figure 1). The tide gauge data has been taken from the World Sea Levels site: https://webcritech.jrc.ec.europa.eu/SeaLevelsDb/. At each location, the mean elevation has been removed from the observations. The comparison shown here is for the 3-way coupled model ('Sequence 2', with WCI included) for the period 2nd to 16th May 2018 covering a spring-neap tidal cycle.

The match between the observed and modelled tidal elevations is quite good, though not perfect. In practice, the comparison is sensitive to the locations used to extract the predicted tidal heights, since the modelled bathymetry may not be sufficiently well resolved at the precise tide gauge locations. Both tide gauge data and model predictions have been harmonically analysed using the Matlab 't_tide' Tidal Analysis Toolbox (Pawlowicz et al., 2002), with a focus on the dominant M_2 constituent, and also the S_2 constituent (smaller by a factor of more than 3). At Holyhead the respective observed and predicted M_2 amplitudes are 1.81 m and 1.68 m (difference 7.0%) and phases are 290.8° and 293.6° (difference 2.8°), with the predictions slightly lagging the observations. The respective results for S_2 are, for amplitude, 0.58 m and 0.52 m (difference 11.2%) and, for phase, 315.5° and 337.8 (difference 22.4°). At Llandudno the respective observed and predicted M_2 amplitudes are 2.72 m and 2.61 m (difference 3.9%) and phases are 308.3° and 318.4° (difference 10.1°). The corresponding results for S_2 are, for amplitude, 0.83 m and 0.79 m (difference 4.3%) and, for phase, 338.5° and 8.1° (difference 29.6°). These results for the tide gauge locations provide satisfactory agreement, particularly for the dominant M_2 constituent.

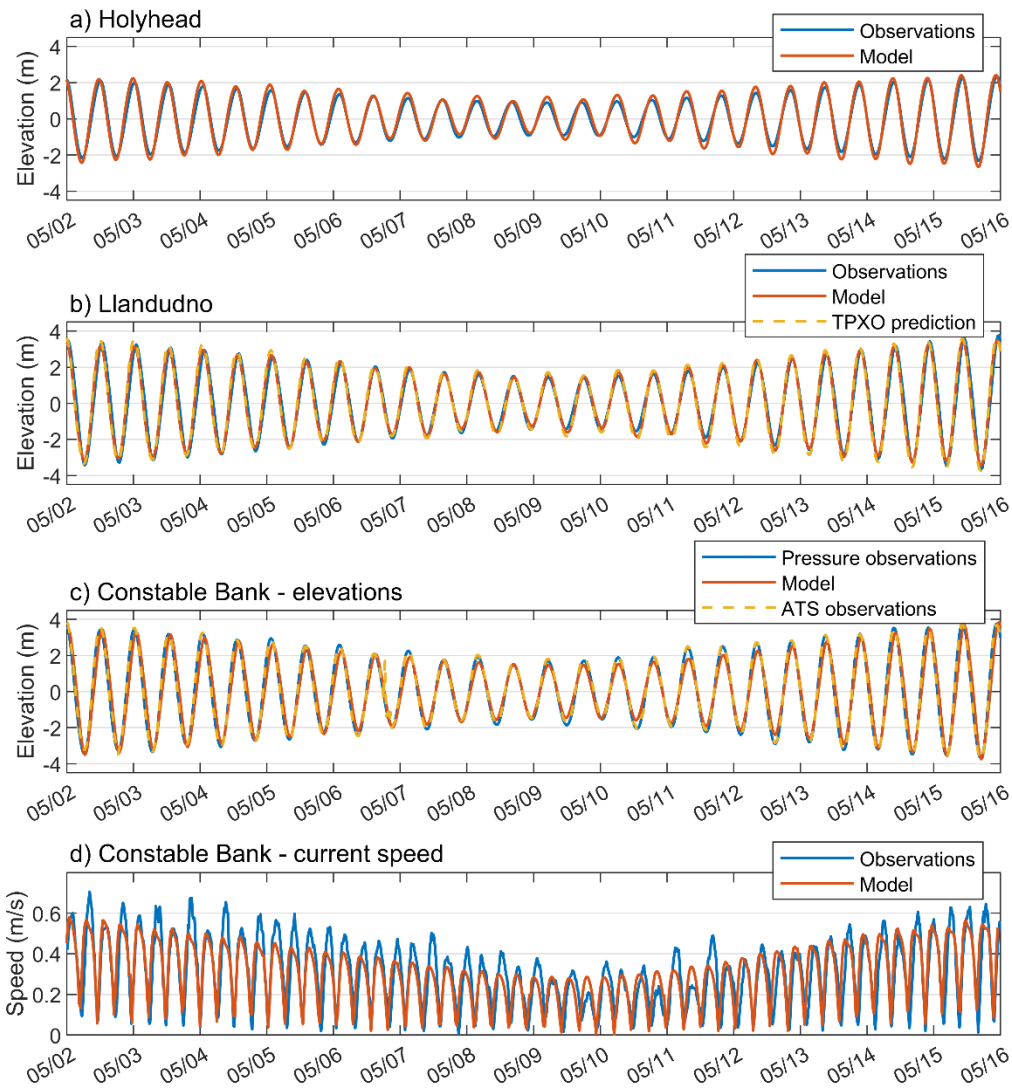

Fig. 3. Validation sequence for simulated tidal elevation at (a) Holyhead, (b) Llandudno and (c) Constable Bank, for 02-16 May 2018. The Llandudno sequence includes a TPXO solution from a full Irish Sea model. Observations in (c) were obtained from both pressure and from an acoustic AST measurement. The corresponding validation comparison for observed and simulated depth-mean current speed is shown for Constable Bank in (d).

Minor discrepancies, day-by-day, may have arisen due to wave effects on tidal heights and/or due to the adequacy of using only 5 tidal constituents. In order to assess this latter point a validation run was conducted for May 2018 using 13 primary harmonic constituents (M_2, S_2, N_2, K_2, K_1, O_1, P_1, Q_1, M_4, MS_4, MN_4, M_f and M_m), derived from the Topex/Poseidon TPXO global tidal database on a structured grid of 0.25° resolution (Egbert et al., 1994). Both surface elevation variation and the deduced horizontal velocities were used at the model boundaries. Previous Telemac modelling studies have implemented boundary conditions based on TPXO data, providing validation of its

accuracy in the Irish Sea (Piano, et al, 2017; Demmer, et al., 2022). Model results based on TPXO data are included in Figure 3(b) for the Llandudno tide gauge location. Both model solutions lag somewhat behind the observed tidal height at HW and the same is true for the TPXO solution at LW. The comparisons in Figure 3(b) provide a context for those made below with the AWAC Frame 1 data recorded on Constable Bank.

The AWAC Frame 1 (see Figure 1) provided two estimates of water surface elevation: i) from pressure measured on the frame at a height of 1.3 m above the seabed and ii) from acoustic AST (Automatic Surface Tracking) measurements of distance to the sea surface made at the same height. Pressure has been converted to height assuming water density 1025 kg/m^3, and both determinations of observed water depth take the frame height into account. The mean elevation has been removed from both sets of observations shown in Figure 3(c) and, the AWAC location being relatively close to that of the Llandudno tide gauge, these results exhibit similarities with those in Figure 3(b). Both observed elevation time series have been harmonically analysed using 't_tide' for comparison with the model predictions. The respective observed (with ATS elevations italicised in brackets) and predicted M_2 amplitudes, are 2.78 m (*2.78* m) and 2.66 m (differences 4.1% (*4.4%*)), and phases are 309.8° (*310.0*°) and 319.7° (differences 9.9° (*9.7*°)), with the predictions slightly lagging the observations, as for the Llandudno results in Figure 3(b). The respective results for S_2 are, for amplitudes, 0.85 m (*0.85* m) and 0.81 m (difference 5.3% (*5.1*%)) and, for phases, 339.8° (*340.1*°) and 9.5° (differences 29.7° (*29.4*°)). The results in Figure 3(c) exhibit reasonable overall agreement with the model results, particularly for the dominant M_2 constituent. It should be noted that the modelled water depths are about 1.4 m less than those observed at the AWAC location; this discrepancy arises from the data sources used to construct the model bathymetry and could probably be improved by exploiting MBES bathymetric information when this becomes available.

The AWAC also provided current velocity determined acoustically. Figure 3(d) shows a comparison between the measured and predicted, depth-mean, flow speed. The AWAC data was integrated to include those acoustic bins of 1 m height lying below the water surface, with an assumed power law velocity profile connecting the lowest bin (centred on 2.7 m above the bed) with the seabed itself. The slight disagreement in the phase of current speed is consistent with that seen for surface elevation in Figure 3(c). More notable is the difference between the magnitudes of the predicted and observed peak speeds. The explanation for this probably lies in the differences between the actual seabed bathymetry and the model bathymetry. In addition, the model simulations exhibit significant spatial changes in the vicinity of the AWAC location; for example, differences in current speed of about 15% occur between locations ±200 m north/south of the AWAC between which the depth varies by 2.8 m, highlighting the uncertainty resulting from the rapid depth variations in the vicinity of the AWAC on top of Constable Bank. As far as flow direction is concerned, the tidal oscillation is highly rectilinear, switching rapidly from about 100°-105°on the flood to about 280°-295° on the ebb. Both observations and predictions exhibit this behaviour, with the model outcome being similar to the example shown later in Figure 10(b).

3.4 Wave input and validation

The waves were implemented in *tomawac* as boundary information comprising significant wave height (H_s), peak period (T_p) and wave direction, which was updated hourly along the entire open-sea perimeter of the model domain shown in Figure 1, an approach similar to that adopted by Luo et al. (2014). This boundary wave input was taken from observations made by the Irish Weather Buoy M2 (location shown in Figure 1) (Marine Institute, 2020) which were assumed to be representative of the entire shelf sea area. The introduction of waves in this schematic fashion at the boundaries of the domain provides a realistic, though approximate, representation of the time-varying wave field in the study area. The justification for this approach is that tidal effects are predominant in most of

the region of interest (apart from the coastal margins), and so waves have been investigated here mainly as a perturbation to this tidally-dominated state.

The observed and modelled outcomes at the M2 location are shown for May 2018 in Figure 4(a) & 4(b). The wave heights here are closely similar, as expected (RMSE for H_s is 0.41 m corresponding to 13.2% of the peak observed H_s); but they are not identical due to minor spectral-evolution of the waves between the boundary of the domain and the M2 location within the domain. The peak periods also show convincing agreement (RMSE for T_p = 0.62 s corresponding to 16.0% of the mean observed T_p for the entire 30-day record).

In contrast, at the AWAC Frame 1 location on Constable Bank, the observed and modelled wave heights show some differences, particularly for days 18 to 20, the modelled wave heights tending to be larger than measured (Figure 4(c)). But the overall agreement seems acceptable, and the same is true for the peak wave period in Figure 4(d) (here RMSE values are not readily calculated due to the observations having a non-constant timestep). The greater variability evident in T_p in the shallower conditions on Constable Bank compared with the deeper M2 location is due to wave interaction with the bank in the rapidly changing water depth. It is possible that, as for the current speed, the predicted wave height is also influenced by the model bathymetry, the modelled water depth in the vicinity of the AWAC being smaller than observed. However, the differences probably also reflect some uncertainty arising from the wave boundary condition, though the assumption of a single, hourly, wave description for the entire open-sea boundary does appear to provide a satisfactory overall characterisation of the wave field.

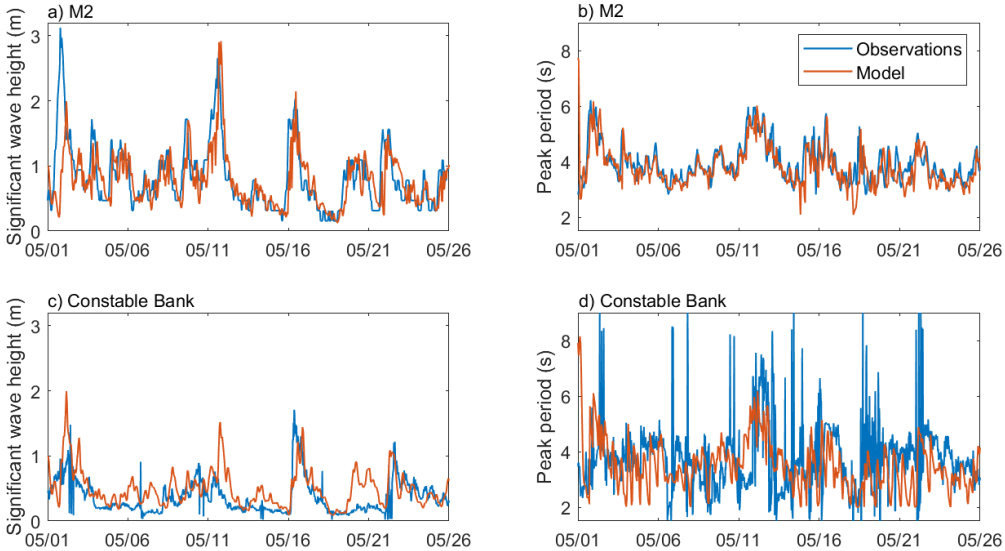

Fig. 4. Model validation of waves for May 2018: Significant wave height (a, c) and peak wave period (b, d), at the M2 buoy location (a, b) and at the AWAC Frame 1 location on Constable Bank (c, d).

3.5 Sediment description and grain size variation

The sediment transport procedures were implemented in module *sisyphe* through several customised user subroutines. A layered seabed structure was introduced which evolves during the simulation. The bed roughness k_s also evolves in time and space as explained below. The aim of the sediment description was to initialize the model with a plausible overall match with conditions on site. Any evolution of the bed and/or mean sediment size predicted during the relatively short-term model simulations can then be used to make inferences about long-term trends in seabed behaviour.

Based on seabed samples in the study area, the bed was defined as having 4 grain size classes with diameters 0.125 mm; 0.18 mm; 1.4 mm; and 10 mm. The 3 smaller sizes were used to define a bimodal bed structure in the mobile sediment bed layer. The bed was further defined as having 3 layers, the uppermost of which (Layer 1) is designated the 'Active Layer', of defined thickness which was taken initially as 0.1 m (for model 'Sequence 2'). This value accommodates the height of typical

small-scale ripples, but it was reduced to 0.04 m in later simulations ('Sequence 2d') to limit mobile sediment availability in the offshore region between Constable Bank and the North Wales coastline.

The 'Active Layer' maintains its defined thickness throughout the simulation, while the thicknesses of the other bed layers change in space and time due to predicted sediment deposition and erosion. Layer 2 is the erodible upper layer which was given initial thickness equal to 0.3 $\times$ local water depth, with its thickness capped at value 5 m. In addition, a minimum initial thickness of 0.5 m was imposed for Layer 2 in shallow areas including the coastal margins. Based on our knowledge of sediment sizes off the North Wales coast, the 4 grain size diameters were initialized in Layer 2 in the proportions 0.23 : 0.30 : 0.47 : 0. Layer 3 is the lower non-erodible layer that occupies the remainder of the seabed down to a base depth of 100 m. Therefore, apart from locations in shallower water, this layer had an initial thickness of 95 m. The 4 grain diameters in Layer 3 were defined in the proportions 0 : 0 : 0 : 1, such that this layer has the largest grain size (0.01 m = 10 mm) corresponding to immobile cobbles.

Sediment transport taking place in the 'Active Layer' was modelled using Bijker's (1992) transport formulation which includes wave effects. This formulation is based on fundamental principles of sediment transport and, while it is relatively simple, it has been found to have the correct general behaviour throughout the parameter ranges of tidal currents combined with waves encountered in the marine environment (Davies and Villaret, 2002). The Bijker transport model includes a suspended load implemented here in a 'local equilibrium' manner (and not, for simplicity, by way of the advection-diffusion scheme available in *sisyphe*). Selective transport of the respective grain fractions occurs in the 'Active Layer' and the aggregated transport (bed load and suspended load) gives rise to seabed evolution. At the end of the 30-day simulation reported here, and without WCI included in the model formulation, localized zones of accretion and erosion (maximum bed evolution

of O(0.5 m)) were predicted quite close to the North Wales shoreline. However, much of this local variation was suppressed when the model was re-run with WCI included.

Selective transport of the grain fractions results in changes to the aggregated mean bed-surface grain diameter. Where significant erosion occurs, especially in the nearshore areas, the grain size composition of the 'Active Layer' alters successively through fractional transport inequalities, which can combine with mixing of sediment down into lower Layer 3 in a so-called 'Active Stratum'. Figure 5(a) shows the variations in mean grain diameter predicted at the end of the simulation for May 2018. Grain size variations are predicted to occur throughout the domain, but a marked trend can be identified for Constable Bank, namely a coarsening on its south side and a fining trend on its north side, in agreement with observations on site. Although these variations occur around the initial mean grain size (0.741 mm), the sediment size on the bed is bimodal with no individual grains having this central (median) size.

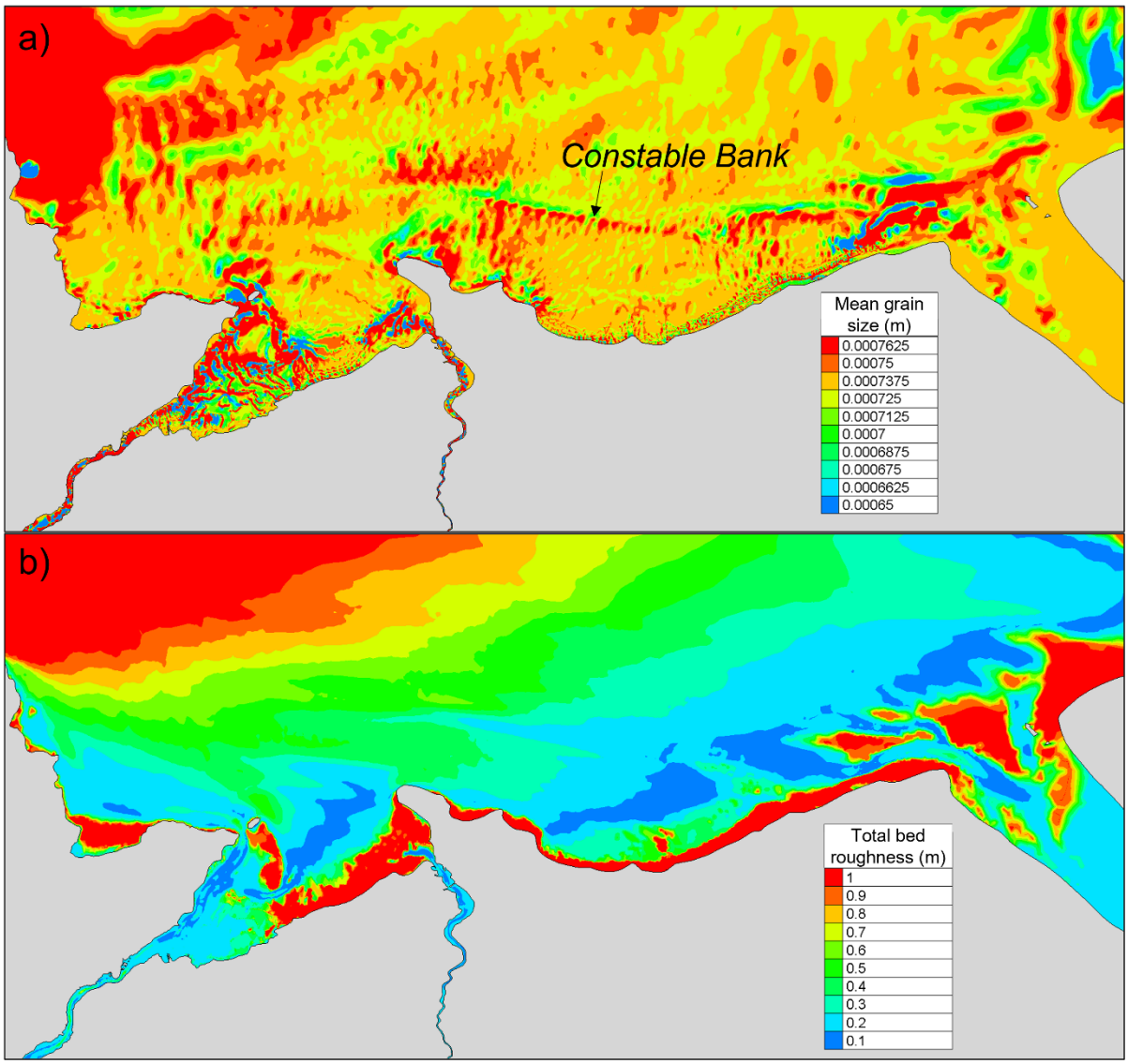

Fig. 5. (a) Mean grain size variation (m) at the end of the 28-day (May 2018) model (Sequence 2) simulation for the North Wales coastal area, with Constable Bank highlighted. Coarsening of the seabed surface occurs in the red areas and fining in the green areas. (b) Total physical bed roughness k_s (m) predicted at the end of the 28-day simulation (May 2018) without WCI included.

3.6 Bed roughness formulation

The frictional influence of the seabed on the tidal flow in shelf seas and estuaries is usually modelled via a prescribed, spatially/temporally invariant drag coefficient. However, the seabed exhibits considerable variability, particularly spatially, that should in principle be included in simulations. Local variations in the seabed roughness (k_s) alter the flow strength and, hence, local sediment transport rates. A spatially/temporally varying k_s was used here extending the method of Davies and

Robins (2017) by the inclusion of wave effects. The main contribution to k_s is made by dunes which are modelled using Van Rijn's (2007) formulation supplemented by a 'history effect'.

Van Rijn's (2007) procedure determines the local value of k_s directly from the predicted sediment grain size, the flow strength (represented by the 'Mobility number' for combined waves + current) and the water depth. In the present implementation, module *sisyphe* predicts the changing total k_s due to the combined effects of sand grains, small-scale ripples, mega-ripples and dunes. The time-varying total k_s calculated by *sisyphe* is fed back into *telemac2d* (see Figure 2). This procedure is accompanied by a relaxation time, or 'history effect', designed to prevent unduly rapid variations in the dominant dune component k_{sd} during tidal cycles, but still allowing a slow modulation in k_{sd} during the spring-neap cycle, moderated by wave effects. The procedures used, which were presented by Davies and Robins (2017), are summarised in Appendix A. The total roughness k_s is further partitioned in *sisyphe* such that only the small-scale ripple roughness k_{sr} is used for local sand transport computations. This approach was validated by Davies and Robins (2017), at least in the absence of waves.

An example of total physical k_s (i.e., without WCI included) at the end of the 28-day simulation for Sequence 2 (May 2018) is shown in Figure 5(b). In the deeper offshore areas, k_s achieves values of 0.9-1.0 m; dune roughness k_{sd} is capped at value 1.0 m in Van Rijn's (2007) formulation. In the shallower areas towards the North Wales coast the value of k_s decreases markedly, before increasing again to large values of order 1 m in the nearshore zone. Here wave shoaling and breaking influence the Mobility number causing an increase in k_s, before a further sharp decrease in k_s occurs towards dry land.

Examination of the individual components of the total k_s in Figure 5(b) shows that the dune roughness component k_{sd} dominates the total, aggregated roughness which is therefore closely

similar to k_s itself. The aggregated result in Figure 5(b) is the quadratic sum of the roughness components predicted for sand grains, small-scale ripples, mega-ripples and dunes. Intra-tidal variations occur in k_s, but these are relatively small as shown by Davies and Robins (2017). It is worth noting that the 'roughness' k_s is fundamentally a representation of the turbulence and mixing in the flow. It is simply a matter of convenience and convention that we attempt to link the 'roughness' that the flow encounters to the size and shape of the physical features (dunes etc.) on the bed. Van Rijn (2007) presented a formulation for k_s itself and then indicated how this might be linked to bed form heights. This latter step forms part of the validation in what follows.

3.7 Validation of bed roughness procedure

MBES data collected by Bangor University has been used for validation of the bed roughness procedure. The MBES data was obtained in both 2017 and 2018, including along the 10 transects shown in Figure 1, and has been compared with modelling outcomes for May 2018. Although the MBES data collection periods and the modelling outcomes are not synchronous, the consistency between the MBES results for 2017 and 2018 suggests that this is not a serious compromise.

MBES observations were logged every 0.5 m along the respective transects shown in Figure 1. Of particular interest initially was the Constable Bank Transect 1, 32 km in length with water depth decreasing from about 25 m at its western seaward end to about 6 m at its eastern shoreward end. However, the greater challenge to the modelling set-up came from the region between Constable Bank and the North Wales coastline due to the mobile upper bed layer (Layer 2) being far thinner in practice than was assumed for initial model simulations (Sequence 2) giving rise to results such as shown in Figure 5(b).

The MBES data logging spatial-interval of 0.5 m allowed dune-scale features to be identified while excluding smaller bed features. In order to extract the dune roughness from the observations, the

MBES data was filtered, using a box-car window, allowing the mean bed level to be removed, leaving only the bed forms on a roughly horizontal base level. These bed forms were Fourier analysed in order to remove two-point instabilities, and the reconstituted smoother bed signal was then interrogated in two ways to obtain an estimate of the spatially-varying k_s through: i) identification of individual crests and troughs of bed forms, allowing individual bed form heights to be estimated along the transect, and ii) calculation of the standard deviation (s.d.) of the bed shape in sections typically 100-400 m long, allowing bed form height to be calculated as $2\sqrt{2} \times$ s.d. for each section. For dunes and mega-ripples, Van Rijn (2007) stated that the roughness is equal approximately to *half the bed form height* and this assumption has been adopted here.

Figure 6(a) shows bed form heights and k_s estimates (Sequence 2) for the Constable Bank transect. The larger size of the bed forms in deeper water at the western end of transect is evident despite large variability in the individual bed form heights (shown by the dots). The bed form heights are smaller in the shallower water along the top of the bank to the east. The envelope of the dots is quite well picked out by the estimate of bed form height made from the standard deviation of bed shape (red line), and this latter estimate has been *halved* to give the observed k_s (green line). It is the comparison between the observed and the model estimates of k_s that provides the validation test. Two comparisons are shown in Figure 6(b), one for a tides-alone simulation (yellow line) and the other for a simulation with waves included (orange line). The only point of departure between the yellow and orange lines is in the shallower water at the eastern end of the transect. The overall agreement in Figure 6(b) between model and observation is convincing.

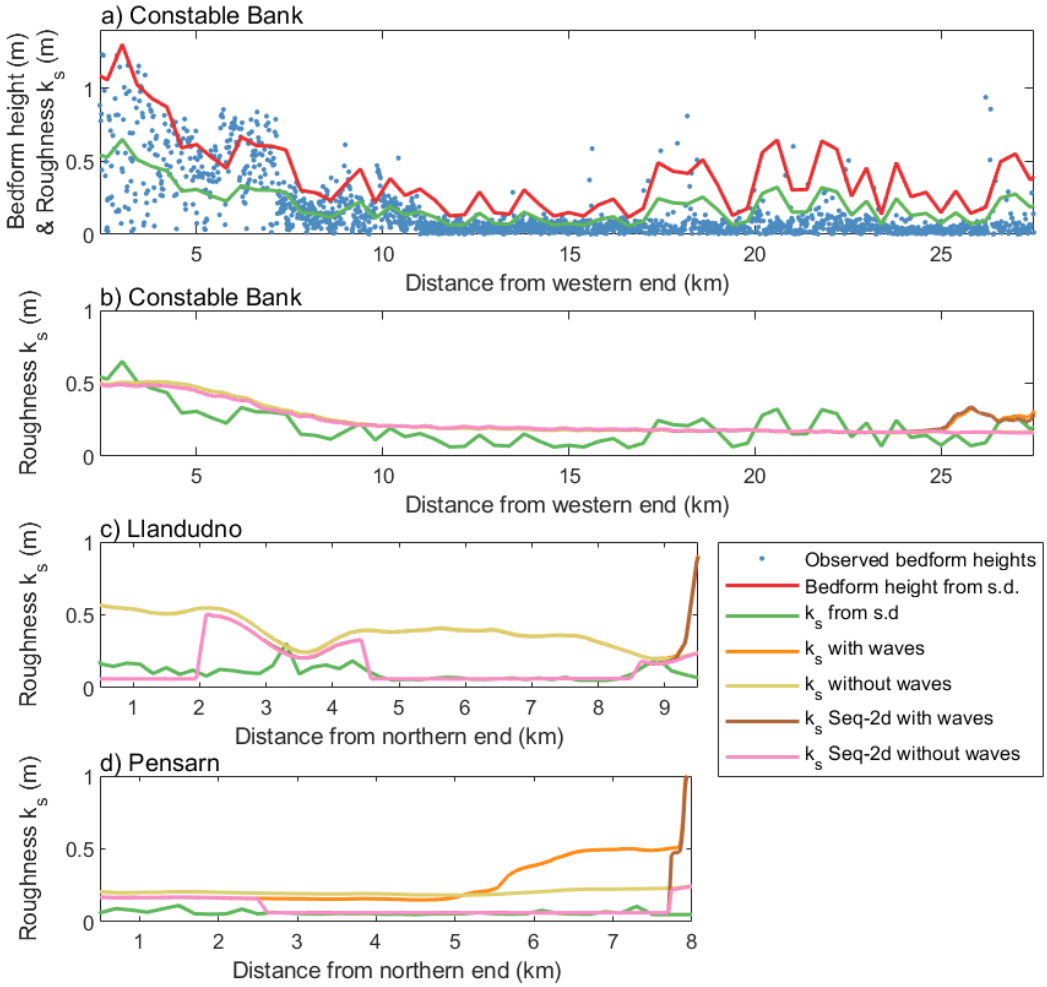

Fig. 6. Comparison between observed bed forms, predicted roughness k_s and model k_s outcomes. (a) Constable Bank transect showing individual bed form heights (blue dots) and heights determined from the s.d. for transect sub-sections of length 400 m (red line), with these values *halved* to give the observed k_s estimate (green). (b) Constable Bay transect showing k_s from the s.d. (green line), with the following model outcomes for k_s at the end of the 28-day simulation for May 2018: k_s for Sequence 2, with and without waves (orange and yellow lines, respectively), and final k_s results for Sequence 2d, with and without waves (brown and pink lines, respectively) obtained after limiting the sediment mobile layer thickness, and also capping the value of k_s, between Constable Bank and the North Wales coastline. Results equivalent to those in (b) are shown for (c) the Llandudno transect and (d) the Pensarn transect.

Figure 6(b) confirms the good agreement between model ('Sequence 2' with and without waves included) and observations for Constable Bank, but far worse agreement occurs along representative transects running across the bank towards the North Wales coastline (Figures 6(c) and 6(d)). The Llandudno transect shows good agreement in k_s across the bank itself and close to the shore, but in between there is a very large discrepancy between the yellow and green lines. A similar discrepancy

occurs for the Pensarn transect. The k_s predictions shown in Figure 6 by the yellow and orange lines assume a fairly deep mobile sediment layer (Layer 2) and it is this assumption that is largely responsible for these discrepancies.

Figures 6(b), 6(c) and 6(d) include further results ('Sequence 2d' with and without waves included) obtained to address the issue of sediment supply based on a set of sub-zones around, but not including Constable Bank. In these zones, upper mobile Layer 2 was assumed to have a reduced initial thickness 0.05 m, with the 'Active Layer' thickness taken as 0.04 m. In addition, the dune roughness k_{sd} was capped for consistency at the value of the thickness of Layer 2 (0.05 m), which is a representative roughness value according to the observations. The consequences for k_{sd} of this approach leave the roughness on Constable Bank, and in the near-shoreline areas, largely unaffected (Figure 6(b)). In contrast, the results shown by the brown and pink lines in Figures 6(c) and 6(d) show a marked reduction in the predicted k_s value between Constable Bank and the shoreline and much more convincing agreement between the observed and modelled roughness values. Lower friction in these defined area leads to somewhat increased flow speeds and, in turn, to adjustments to the predicted k_s throughout the model domain; this can be seen, for example, where the Llandudno transect intersects Constable Bank in Figure 6(c). However, these k_s-adjustments are quite small and do not give rise to any major qualitative changes in the results in Section 4.

Close to shore in Figures 6(c) and (d), the differences between observation and predicted k_s, arising both with and without waves in Sequence 2d, are due mainly to the Layer 2 thickness and the 'Active Layer' thickness returning here to their unadjusted (Sequence 2) values. Reduced thickness for Layer 2, and an 'Active layer' thickness of 0.04 m, could have been assumed right up to the shoreline and this would probably have improved the comparison. The differences between the present simulations with and without waves are most likely due to issues surrounding sediment supply,

rather than poor modelling of wave effects. At the present stage of this research however, site information on the actual thickness of the mobile sediment layer near to shore is unavailable.

4. Model results

4.1 Wave effects on nearshore residual velocity and sediment transport

The role of waves superimposed on the spring-neap tidal motion is potentially significant in relation to both the generation of nearshore currents, and also residual water flux and sediment transport pathways. When wave heights are significant the model predicts that eddy structures form in the region of the breaker zone, with a reversal of current direction sometimes occurring across the breaker line. Such effects are influenced by WCI at the seabed which increases the roughness encountered by the flow particularly in shallower coastal areas. The enhanced friction due to WCI tends to suppress nearshore eddy activity, though this is an aspect of the modelling that requires validation through observations on site (which are presently not available).

As noted in Section 3 (and Appendix A), module *sisyphe* predicts the total physical k_s by combining the effects of sand grains, small-scale ripples, mega-ripples and dunes, with the dominant dune component k_{sd} being subject to a 'history effect'. As far as WCI is concerned there is uncertainty as to whether some, or all, of these physical k_s components should be included in the calculation of the roughness enhancement. This is discussed in Appendix B. The present implementation of WCI includes all three bed k_s components and can therefore be considered as a limiting case representing the most severe level of WCI possible through application of Soulsby and Clarke's (2005) method. The effect of WCI is explained further in Section 5.

In the comparisons that follow the focus is on the residual flow and sediment transport obtained for the k_s description referred to earlier as Sequence 2d. Figure 7(a) shows the residual velocity in a subdomain offshore of the coastal promontory at Llanddulas (defined in the inset) which affects the

dynamics locally. At a point 1 km offshore (at the outer end of the transect used later in Figure 14) in water of mean depth 6.0 m, Figure 7(c) shows the significant wave height (H_s), wave direction (Dir) and peak wave period (T_p), predicted during the 28-day model sequence, during which the mean, maximum and minimum values are, respectively, for H_s (0.40, 1.46, 0.07) m, for Dir (152°, 195°, 124°), and for T_p (3.2, 6.3, 2.0) s. The residual velocity in Figure 7(a) is shown both with and without waves included, as green and red vectors, respectively. The superimposed colour map shows the difference between the residual velocity magnitude with waves minus the magnitude without waves, without regard to flow direction. To the east of the promontory the residual velocity is towards the northwest with the presence of waves suppressing the velocity somewhat (dark blue shading), consistent with the waves being incident from the NNW direction on average. Without waves present the residual achieves values approaching 0.07 m/s; with waves present the residual falls to about 0.05 m/s. To the west of the promontory a counter-clockwise eddy structure occurs in the residual velocity field, which is fully formed without waves, but less complete with waves present. A second, weaker clockwise, eddy exists further to the west in the case without waves. The residual velocity to the west of the promontory is towards the southwest, again reduced in magnitude by waves close to shore, but enhanced by waves seaward of this (dark pink area). When this exercise is repeated for the water flux (= velocity × depth) during the 28-day period, the residual flux pattern (not shown) is more regular and does not exhibit eddy patterns to the west of the promontory.

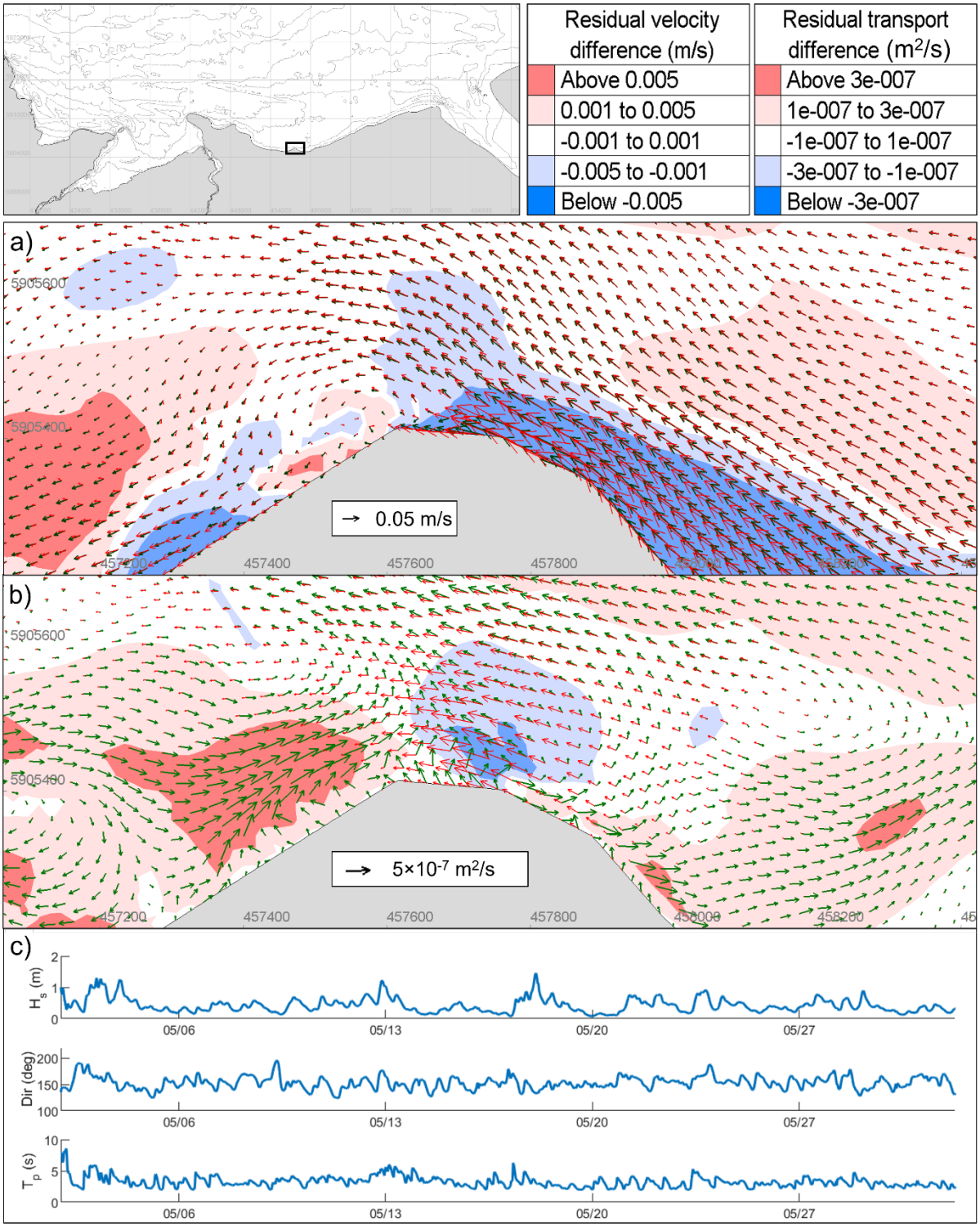

Fig. 7. Residual velocity and sediment transport over 28-day period (May 2018) in the nearshore subdomain off Llanddulas shown in the inset. Here the model resolution is approximately 25 m. (a) shows the residual velocity (m/s) with (green vectors) and without (red vectors) waves included in the simulation. The vector velocity scale is as indicated. The superimposed colour map expresses the difference between the magnitude of the residual velocity with waves present minus the magnitude without waves present, without regard to direction. (b) shows an equivalent plot for residual sediment transport (m^2/s). (c) shows the significant wave height (H_s), wave direction (Dir) and peak wave period (T_p), at a point 1 km offshore in water of mean depth 6.0 m.

The residual sediment transport pattern in Figure 7(b) exhibits some contrasting features. In the absence of waves, the residual transport follows a regular pattern, generally directed towards the west. A more complicated structure results from the presence of waves, including eddies both east and west of the promontory, and with an eastward directed transport near to shore. This residual transport is generally enhanced by waves particularly on the western side of the promontory (pink area).

While eddies are evident in the residual velocity and sediment transport patterns off Llanddulas promontory, these structures are not present in the respective *instantaneous* patterns. The instantaneous vectors are far more regular, following the coastline shape for the most part. In other words, the eddy structures evident in Figure 7 are not likely to be the cause of any related seabed morphological changes. Further, there is no reason to suppose that the behaviour of the flow and transport close to the shoreline has direct impacts offshore. Even if nearshore residual transport eddies were thought to be capable of generating bathymetric changes away from the coast, their persistence in time and space would work against this logic. The very large tidal range in the study area would cause any instantaneous eddy structures to move repeatedly away from and then towards the coastline with the tidal period, smoothing out short-term bathymetric variations.

4.2 Residual velocity and sediment transport near Constable Bank

Figure 8 shows the corresponding 28-day residual velocity field for the Constable Bank subdomain. Here a westward velocity residual (of magnitude up to about 0.05 m/s) is predicted on the south side of the bank and an eastward residual of similar magnitude on the north side. This contrasts with the inference made by Kenyon and Cooper (2005) of eastward-directed residuals on both sides of the bank (see Section 2). While the results shown in Figure 8 are from the simulation with wave effects included, closely similar results are obtained in this subdomain without waves. The differences between residual velocities predicted with and without waves are directed mainly southward across

the top of the bank, i.e., waves slightly inhibit the northward residual across the bank, and are of magnitude at most 0.0005 m/s, that is two orders of magnitude smaller than the residuals themselves in the respective simulations.

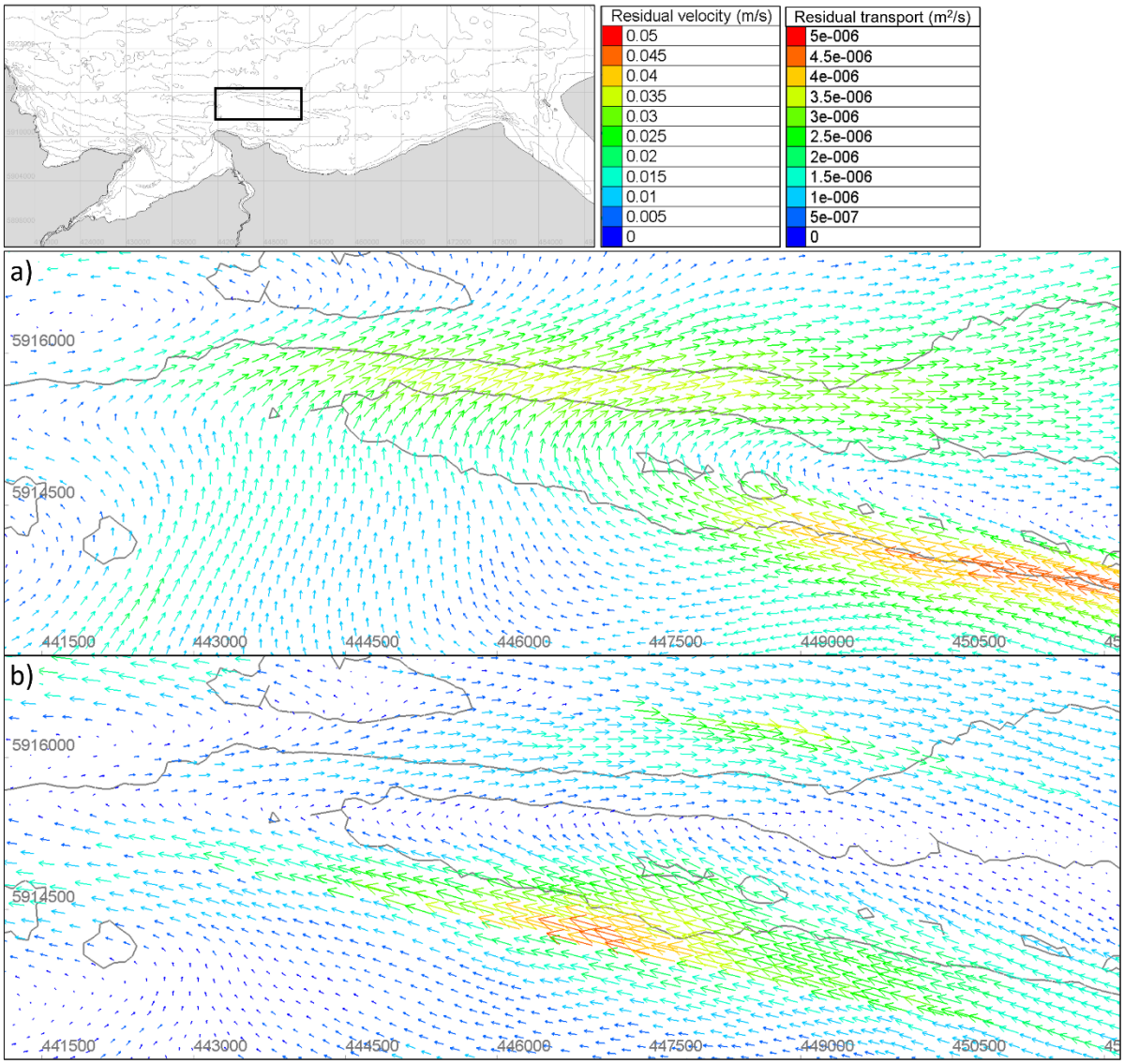

Fig. 8. Residual velocity and sediment transport over 28-day period (May 2018) in the Constable Bank subdomain shown in the inset with waves included in each simulation. The black bottom contours show depths increasing in 5 m increments from 10 m on top of the bank to 25 m at the northwest edge of the subdomain, and the model resolution is approximately 200 m. (a) Residual velocity (m/s) and (b) residual sediment transport (m^2/s) with the respective vector scale as indicated in the legend.

The residual sediment transport vectors shown in Figure 8(b) are an order of magnitude larger than those in Figure 7(b) due to the strong tidal currents occurring offshore. As for the residual velocity a clockwise residual transport is predicted around the end of the Constable Bank, with westward and eastward directed transports of similar magnitude on its south and north sides, respectively. The

peak residual transport in the subdomain is displaced to the west compared with the peak residual velocity in Figure 7(a). The transport results include wave effects, but the (slightly smaller transport) results without waves present (not shown) are strikingly similar. The differences between the residual transports with and without waves, both north and south of the bank, are two orders of magnitude smaller than the transport values themselves. The greatest transport differences arise on top of Constable Bank, but even here they remain smaller by a factor of at least 5 times than the transport residuals. These differences are directed such that the waves cause a small westward adjustment to the residual transport. Overall, waves are shown by the modelling outcomes to have a substantially greater relative effect on the transport than on the velocity.

The close similarity between the residual velocity and sediment transport patterns, both with and without waves present, suggests that the 'clockwise' circulation pattern seen in Figures 8(a) and 8(b) represents the general behaviour around the north-western end Constable Bank. Large storms could disrupt this pattern over short intervals, but the predominant circulation will be dominated by processes occurring over longer time scales of weeks, months and years, involving typical medium-sized waves superimposed on the tidal flows, as found for typical offshore sites by Soulsby (1997) and for the nearshore coastal zone by Soulsby and Malarkey (2005). The results in Figure 8 are consistent also with the observed tendency for Constable Bank to erode on its south flank while accreting on its north flank, an outcome implicit in Figure 5(a).

4.3 Residual velocity in the North Wales coastal area

In order to gain further insight into the residual velocity and sediment transport patterns, a set of 10 north-south transect lines has been defined to encompass the North Wales coastal area including Constable Bank (Figure 9). On each of these lines the west-to-east U-component and south-to-north V-component of the respective residuals have been extracted from the 28-day simulations. The transects have length 20 km and are numbered from T1 in the west to T10 in the east. Transects 2

to 5 cross Constable Bank, and the lower portion of Transect 1 incorporates the outer Conwy Estuary. In addition, a set of instantaneous sediment transport predictions has been extracted at defined locations on these north-south transects (see Section 4.4).

The residual velocity is shown in Figures 9(a) and 9(b) for simulations carried out with and without waves included, respectively. Some small differences can be seen to be caused by wave effects, particularly for the transects on the eastern side of the domain. The results show a westward-directed residual originating in the Dee estuary, which on the 9th transect achieves a maximum speed of 8.4 cm/s in the absence of waves, enhanced to 9.9 cm/s when waves are present. These findings are consistent with the modelling outcomes of Bolaños et al. (2013) for the flow in the Welsh and Hilbre Channels in the Dee Estuary (see Section 5). The residual flow following the shoreline direction weakens, and then splits into two westward directed flows, one close to the shoreline and the other directed along the south side of Constable Bank. On the 4th transect the maximum westward nearshore residual flow speed is about 3.1 cm/s both without and with waves present. Further from shore the residual becomes eastward directed and of magnitude 1.6 cm/s, before returning to westward directed of magnitude 4.1 cm/s on the south side of Constable Bank. The residual on the north side of the bank is in the opposite direction from west to east with maximum strength of 3.3 cm/s, both without and with waves present, with directional changes then predicted on the respective transect lines further to the north.

The results in Figure 9 indicate a clockwise flow circulation pattern around Constable Bank of magnitude a few centimetres per second together with a westward drift close to the coast itself. In the middle of the region between the bank and the coastline, the residual is weak and somewhat indeterminate, but directed mainly eastward. Wave influence on the transect residual velocity profiles nowhere exceeds about 1.5 cm/s; differences due to waves are greatest towards the east

and are generally confined to the nearshore zone. Here the waves tend to give rise to an eastward adjustment to the nearshore residual of ~1 cm/s.

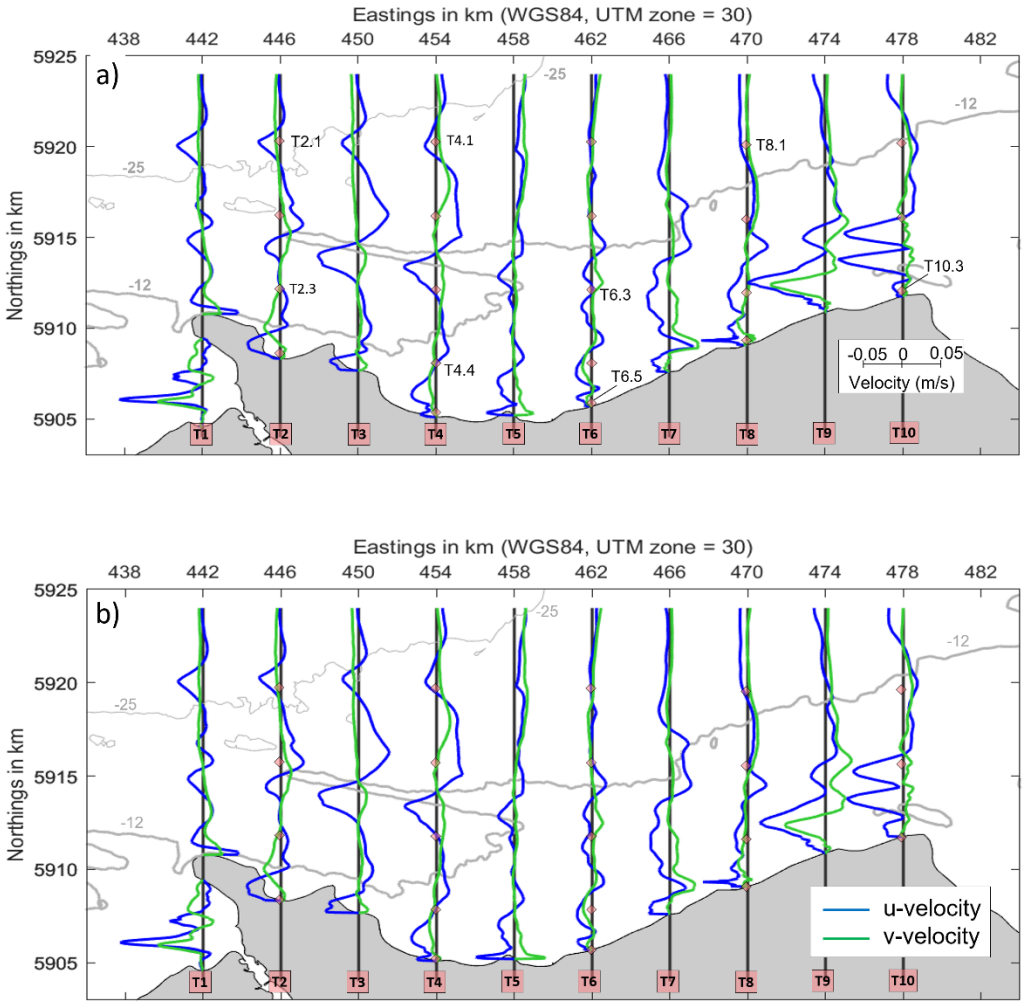

Fig. 9. Residual velocity (m/s) components (west-to-east u-velocity as blue lines and south-to-north v-velocity as green lines) calculated for the 10 NS-transects (vertical black lines, T1 – T10). Results are shown for model Sequence 2d (May 2018) both (a) with and (b) without wave effects included. The velocity scale is as defined in (a). The transects are mapped to-scale spatially (left y-axes and upper x-axes, in km) and superimposed on the North Wales coast (grey shading) and offshore bathymetry (−25 m (thin) and −12 m (thick) contours). Transects T1-T10 have length 20 km and T2 to T5 cross Constable Bank which is highlighted by the −12 m contour. A set of points (red diamonds) are positioned on T2, T4, T6, T8 and T10, e.g., for T2: denoted T2.1 (most northerly point), T2.2, T2.3 and T2.4 (most southerly point), as labelled selectively in (a). These points are used to interrogate the local sediment transport throughout the North Wales coastal domain.

In order to assess the generality of the conclusion that there exists a clockwise residual circulation around the seaward end of Constable Bank, an additional 'hypothetical' simulation was run for Sequence 2d. In this simulation the wave height on the boundary of the model domain was doubled compared with the results shown in Figure 4, with all other inputs including wave period and direction unaltered. This adjustment gives rise to waves at the upper end of the range of wave heights observed in Liverpool Bay, as reported by Wolf et al. (2011) (see Section 2). In comparison with the residual velocity strengths quoted above, on the 9th transect the westward directed flow was enhanced by ~1 cm/s, achieving an increased maximum value of 10.8 cm/s. In contrast on the 4th transect, the residual velocities on both north and south sides of Constable Bank differed from results quoted earlier by only 1 mm/s or so, confirming the dominant influence of the tides and the relatively small importance of the waves in determining the residual flow.

In summary, the similar results in Figures 9(a) and 9(b), supported by the hypothetical simulation, confirm the clockwise, tidally dominated, circulation pattern around the western end of Constable Bank to be a robust finding, albeit from modelling rather than observation. Wave effects are greatest on the three eastern transects (T8, T9 and T10), giving rise here to an easterly residual contribution close to the shore, but a more variable pattern offshore. Close to the North Wales coast there is a very small eastward drift in general while, further out to sea and in the region of Constable Bank, wave effects are of little consequence to the residuals. The wave effects that do occur are predominantly due to enhanced wave-induced friction encountered by the currents offshore, and due to currents induced by waves near to shore.

The residual velocity patterns in Figure 9 give only an impression of relative flow strength. They do not account for changing water depth and so do not coincide with the residual water flux (i.e., velocity $\times$ water depth) patterns. However, these patterns (not shown) have been found to be

qualitatively similar in respect of the clockwise circulation around Constable Bank. The corresponding calculations shown next for residual sediment transport do not involve this ambiguity.

4.4 Wave effects on predicted instantaneous sediment transport rates

By way of introduction to the *residual* sediment transport results, some examples of *instantaneous* sediment transport predictions provide insight into the magnitude of the residuals. Instantaneous transport rates are presented for selected locations lying on the NS-transects shown as red diamonds in Figure 9(a). As a representative period during the 28-day model Sequence 2d, Days 15 and 16 (Hours 336 to 384) were selected during which significant wave activity developed during the second day. The 48-hour time-series in Figure 10 are of the instantaneous sediment transport rate at points T2.3, T4.4 and T6.3. The peak velocity during this period displays an alternating ebb-flood variation while increasing somewhat in magnitude in successive ebb and flood cycles. The wave height is low during Day 15, but increases significantly during Day 16, with the sediment transport rate being influenced by wave effects. At each of the 3 locations shown in Figure 10, results are presented for the magnitude of the predicted sediment transport rate, together with a polar plot expressing additionally the transport direction, for tides alone (red), for tides with waves (green) and for tides with 'hypothetical' waves of doubled height (blue).

Point T2.3 on the second transect illustrates the growing influence of waves on sediment transport during Day 16 (Figure 10(a)). Here the water depth range during the 48-hour period was 11 to 19 m. For waves with the observed peak period $T_p \sim 4$ s, this implies a surface wavelength of about 25 m which results in relatively little near-bed wave activity. However, the nonlinearity of the sediment transport process is still evident, with the doubling of the wave height in the later cycles (blue curve) having a much greater proportional effect than occurs for the simple addition of (unaltered) waves (orange curve) to the tides (red curve). The vector plot (Figure 10(b)) shows the transport pathways

to remain essentially rectilinear at T2.3, and to be consistent with a transport residual directed to the WNW.

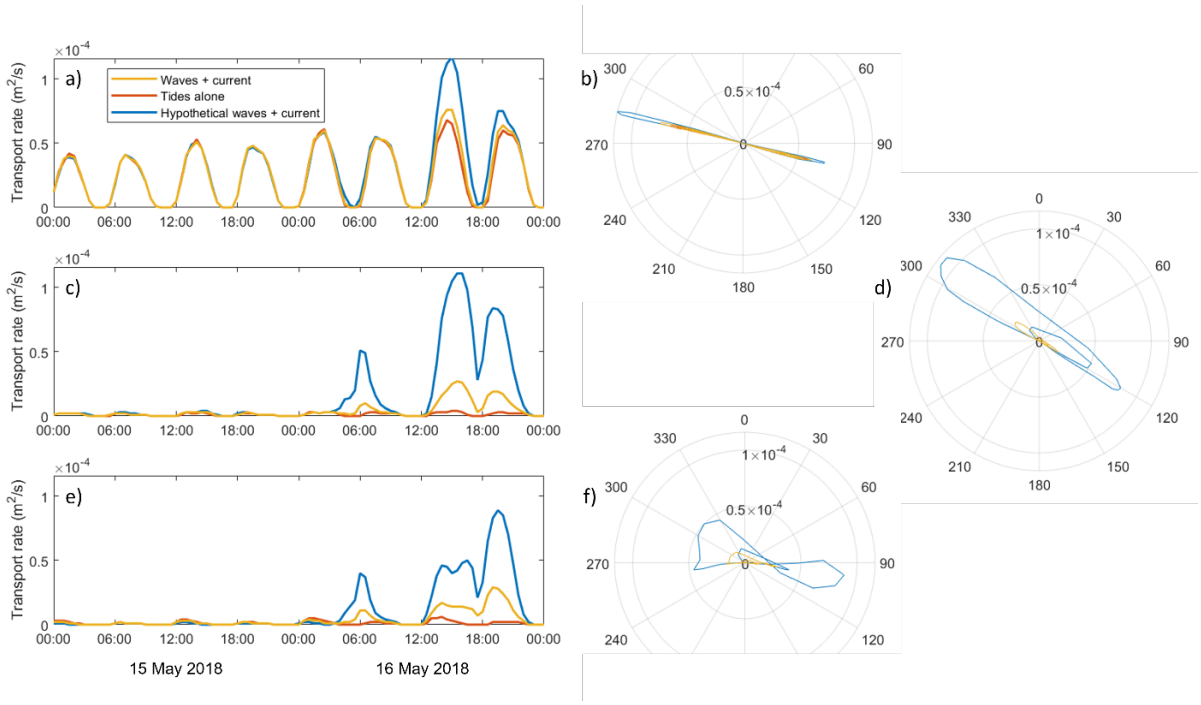

Fig. 10. Sediment transport rate predicted during 15 and 16 May (hours 336-38) of the 28-day model Sequence 2d at (a,b) point T2.3, (c,d) point T4.4, and (e,f) point T6.3 (see Figure 9(a) for reference). (a), (c) and (e) show time series of the magnitude of sediment transport rate (m^2/s); (b), (d) and (f) show transport rate (m^2/s) in a polar view at the respective points. Transport rates are shown for tides alone (red), waves + current (orange) and hypothetical waves + current (blue), with WCI included.

Point T4.4 shows results at a shallower location on the fourth transect (depth range 4-13 m) (Figure 10(c & d)). Here tidal currents alone produce very little transport, while the addition of waves enhances the transport significantly, particularly for the hypothetical waves, as expected. The transport vectors here follow a more elliptical pattern, but still NW-SE directed, following the shoreline orientation.

In the centre of the domain at point T6.3 (depth range 3-12 m), which lies on the connection between Constable Bank and the coast, the results in Figure 10(e & f) show little transport associated with tides alone, but significant transport when waves are present. The transport 'butterfly vector' is here quite broad, lying along a WNW-ESE axis.

The instantaneous sediment transport magnitudes at the three locations shown in Figure 10 achieve values of up 3×10^{-5} m^2/s for tides alone, values in the range 3×10^{-5} to 8×10^{-5} m^2/s for tides combined with (unaltered) waves, and in the range 8×10^{-5} to 12×10^{-5} m^2/s for tides combined with 'hypothetical' waves. Such values can be compared with the residual transport values quoted in what follows.

4.5 Residual sediment transport in the North Wales coastal area

The residual sediment transport patterns for the 10 north-south transects are shown in Figure 11 for the 28-day simulations, with (11(a)) and without (11(b)) wave effects included, together with the difference (a) minus (b) shown in 11(c). Since the 12 m depth contour highlighted in Figure 11 corresponds to about one half of the representative surface wavelength (quoted earlier), this contour delineates quite well the region in which wave effects become significant at the seabed. Although wave influence is more pronounced for transport than it was for residual velocity, it again does not influence the overall residual transport patterns in Figure 11 significantly.

The results in Figure 11 show a complicated picture on the 10th (most eastern) transect for the residual transport originating in the Dee estuary, but by the 9th transect a more orderly pattern is established. Here in the absence of waves, the maximum westward directed transport is -4.3×10^{-6} m^2/s. When waves are present, this value almost doubles to become -7.7×10^{-6} m^2/s to the west. This illustrates the additional stirring effect of the waves which significantly enhance the transport of sediment by the current. Between Constable Bank and the shoreline, a general pattern of a small westward residual transport then becomes established. On the 2nd transect the maximum westward residual on the south side of the bank (U-comp) is -3.3×10^{-6} m^2/s, while the maximum eastward value on the north side (U-comp) is 1.4×10^{-6} m^2/s, with waves present in each case. These values correspond to −0.0087 and 0.0037 kg/m/s with an assumed sediment density of 2650 kg/m^3. These

are relatively small transport values as would be expected for residual estimates (c.f. the instantaneous transport outcomes in Figure 10).

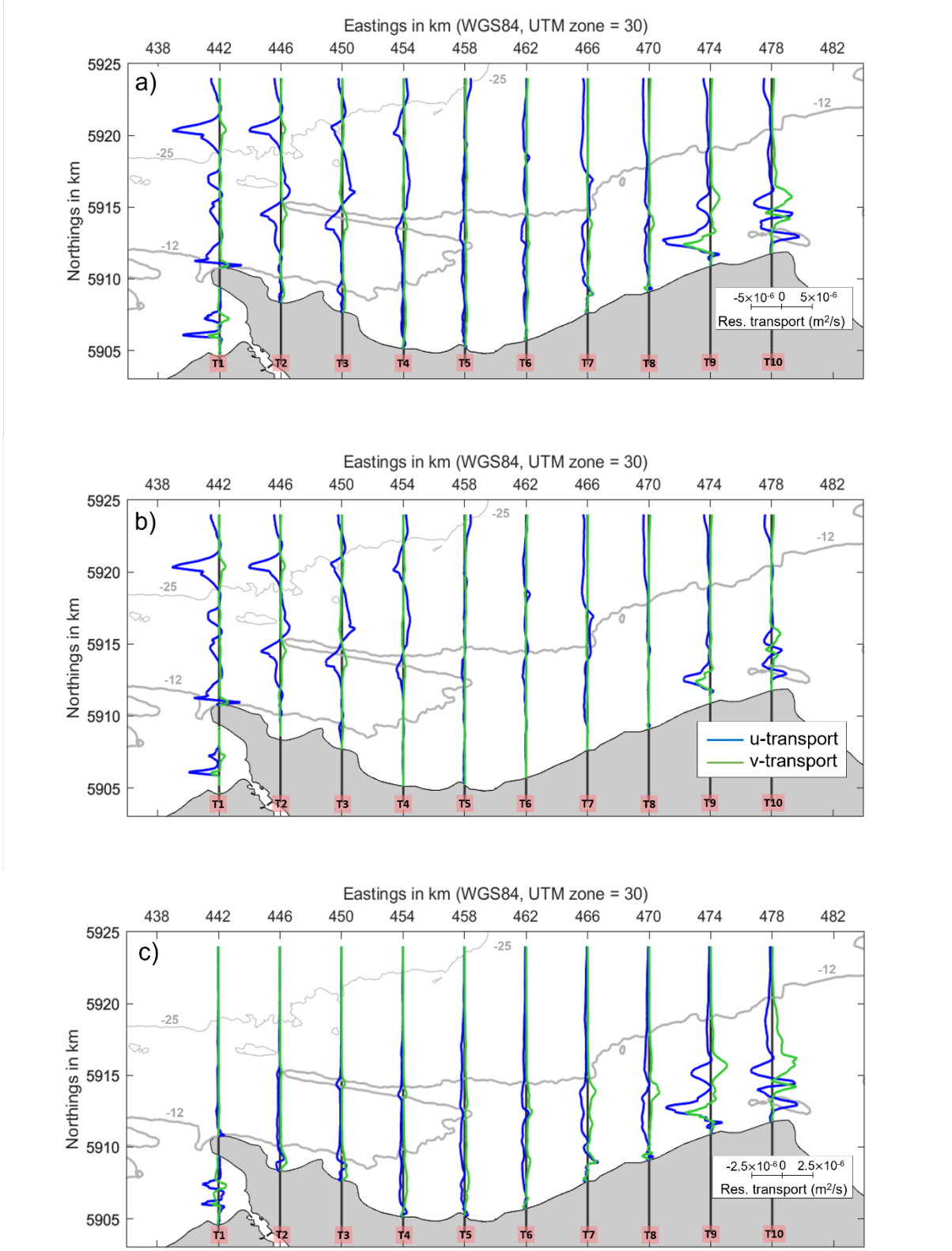

Fig. 11. Residual sediment transport (m^2/s) components (west-to-east u-transport as blue lines and south-to-north v-transport as green lines), calculated for the 10 NS-transect lines (vertical black lines, T1-T10). Results are shown for model Sequence 2d (May 2018) (a) with and (b) without wave effects included, together with (c) the difference (panel-a minus panel-b). The transport scale is defined in (a) for (a) and (b), and separately in (c). The transects are mapped to-scale spatially (left y-axes and upper x-axes, in km) and superimposed on the North Wales coast (grey shading) and offshore bathymetry (−25 m (thin) and −12 m (thick) contours).

The differences in Figure 11(c) between the residual transports with and without waves, both north and south of Constable Bank, are two orders of magnitude smaller than the transport values themselves. Through most of the domain, including over Constable Bank, the effect of waves is to promote residual transport towards the north and west, though by only a very small amount. Close to shore the pattern is more confused, with waves tending to enhance eastward transport on the western transects, and to enhance westward transport on the eastern transects, though with a mainly northerly tendency on all transects indicating that the waves are predicted to contribute to net offshore residual sediment transport.

In an overall sense the transport results for May 2018 again indicate a clockwise pattern around the offshore end of Constable Bank together with a generally westward drift between Constable Bank and the North Wales coast. This small westward drift extends close to shore on the first 7 transects but is reversed to a small eastward drift close to shore on the 8th and 9th transects. The opposing directions of residual transport (and also velocity) on either side of Constable Bank are consistent with it being a stable bed feature, and here the model outcome helps to resolve the contradiction posed by Kenyon and Cooper (2005); they inferred from observations of the asymmetry of large-scale sand waves that the residual transport and flow was in the *same* direction on both sides of the bank, suggesting that the bank would not survive in the long term.

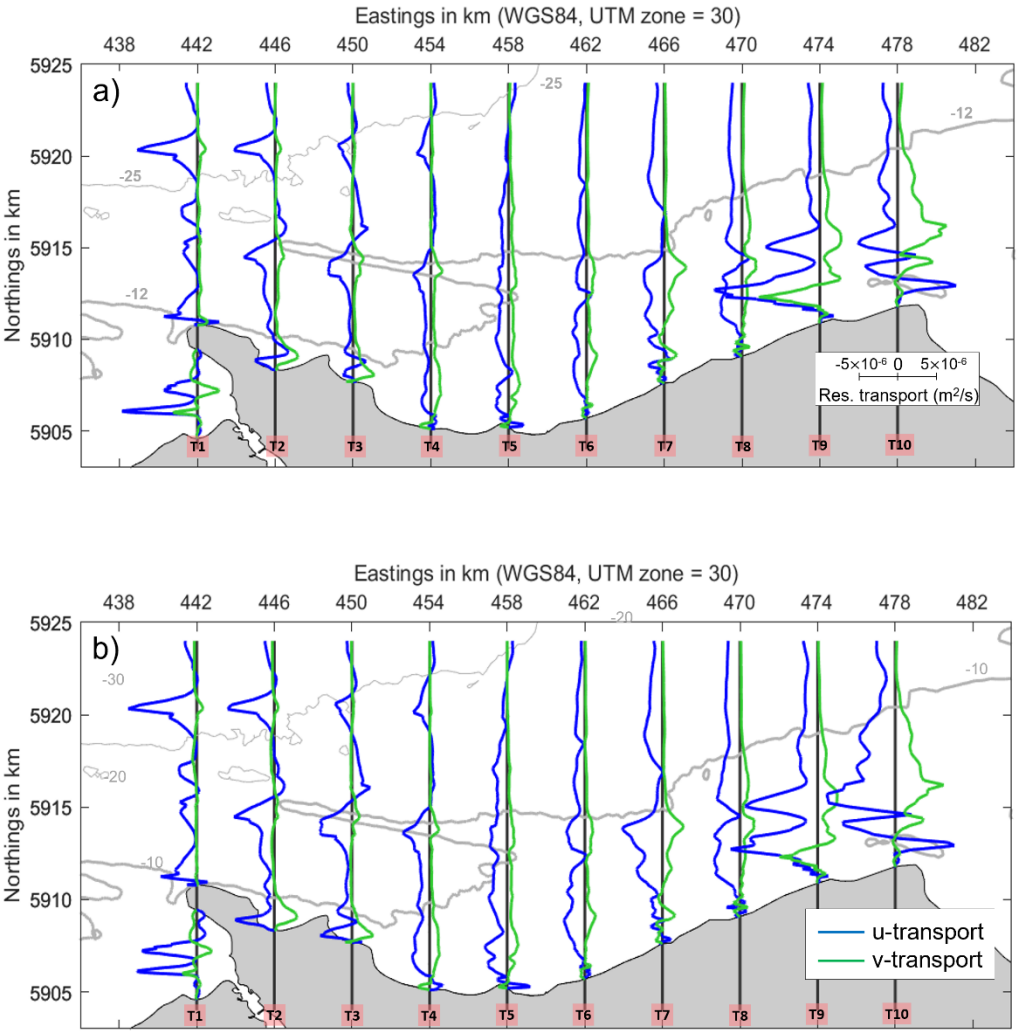

Fig. 12. Residual sediment transport (m^2/s) components (west-to-east u-transport as blue lines and south-to-north v-transport as green lines), calculated for the 10 NS-transect lines (vertical black lines, T1-T10). Results are shown for model Sequence 2d (May 2018) (a) with 'hypothetical' waves of doubled height included and (b) the difference between (a) and the case of tides alone in Figure 11(b). The transport scale is as defined in (a). The transects are mapped to-scale spatially (left y-axes and upper x-axes, in km) and superimposed on the North Wales coast (grey shading) and offshore bathymetry (−25 m (thin) and −12 m (thick) contours).

The generality of the conclusion regarding the clockwise residual transport around the seaward end of Constable Bank has again been assessed using the additional 'hypothetical' simulation carried out for Sequence 2d with wave height on the boundary of the model domain doubled to encompass the full range of waves likely to occur on site. These results are shown in Figure 12(a) and the difference between Figure12(a) minus the case of tides alone in Figure 11(b) is shown in Figure 12(b). In

comparison with the residual transport values quoted above for the 9th transect, the peak westward residual offshore takes the value of -1.35×10^{-5} representing a further significant enhancement in transport by a factor of 3 times compared with the unadjusted wave-current case. On the 2nd transect the effect of the increased wave height is less marked. On the south side of Constable Bank the peak westward residual is -4.0×10^{-6} m^2/s, while on the north side it becomes 1.4×10^{-6} m^2/s. The former value represents a small enhancement of the westward transport due to the larger waves, while the latter shows no such wave effect. More generally these results suggest that the predicted clockwise, tidally dominated, circulation pattern around the western end of Constable Bank is a robust conclusion. The transport differences due to the enhanced waves shown in Figure 12(b) are also much larger throughout the domain than those caused by the unadjusted waves shown in Figure 11(c).

4.6 Sediment transport pathways in greater Liverpool Bay

Much of the earlier literature has suggested a general net, long term, drift of sediment eastwards across Liverpool Bay towards the English coast. While the present model outcomes concur with this, they indicate that local patterns of net sediment drift are quite complicated, particularly in the vicinity of Constable Bank and close to the North Wales coast. Figure 13 shows a colour map of residual transport magnitude in a wider area, together with arrows indicating the associated local transport direction (but not its magnitude). Residual transport magnitudes are predicted to be greatest off the north coast of Anglesey and in the region off the Mersey Estuary though, as noted in Section 5, Brown et al. (2015) showed that baroclinicity limits the residual sediment circulation out of the Mersey, an effect not included in the present barotropic modelling. The westward transport shown north of Anglesey is part of a clockwise cell in which the strong net transport becomes eastward-directed further to the north (out of the view shown in Figure 13). This supplements a strong north-easterly net drift to the west of Anglesey which feeds sediment into Liverpool Bay. In

contrast, transport magnitudes are significantly lower in the central (blue) area, including in the locality of Constable Bank.

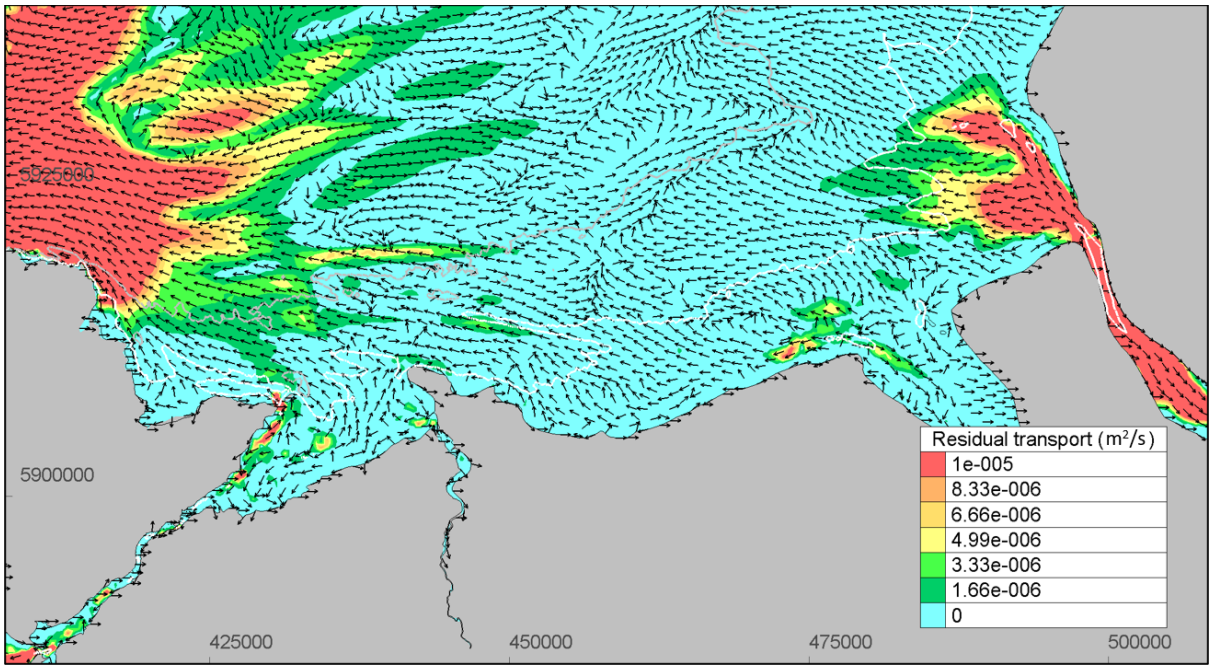

Fig. 13. Colour map of residual sediment transport magnitude (m^2/s), with arrows denoting direction, for model Sequence 2d. The arrows, interpolated on a coarse regular grid, are included without regard to transport magnitude, to give a general idea of the sediment circulation pattern during the 28-day simulation (May 2018). The contours show depths: grey = 25 m and white = 12 m, highlighting Constable Bank.

On the regular grid used in Figure 13 to illustrate the general features of the transport pattern, the arrows indicate a west-to-east tendency in upper parts of the region shown, but with a complicated pattern as the North Wales coast is approached. South of Constable Bank, and throughout much of the region to the east towards the Dee Estuary, a small westward transport residual is evident, as discussed earlier in connection with Figure 11. Although Figure 13 does not resolve nearshore behaviour in any detail, it suggests that the residual transport direction becomes more variable here, with eastward net transport predicted at some of the easterly coastal locations. The processes in the near-coastal area are discussed further in Section 5; these include wetting and drying effects that strongly influence the nearshore residual sediment transport.

5. Discussion

5.1 Wave-Current Interaction (WCI)

The effects of WCI at the seabed occur primarily in the nearshore and are illustrated in Figure 14 for a transect offshore of the Llanddulas promontory (part of Transect 5 in Figure 1). Here WCI, as presently applied (see Appendix B), becomes the predominant effect out to ~350 m from the shore. To demonstrate this, a particular time instant was selected during the simulation: 15 May 2018 at 20:00 hrs; waves were present at this instant propagating beyond the breaker line at ~140° towards the southeast. The tidal current was running eastward across the transect (i.e., a flooding tide).

The effect of WCI at the Llanddulas transect can only be understood with reference to the k_s prescription in the coupled model. It may be recalled from Figure 5(b) that the presence of waves enhances the physical k_s significantly close to the shoreline, while having a lesser effect offshore, with the severity of the applied WCI dictating the magnitude of this k_s enhancement. The physical k_s itself is dominated by the dune component k_{sd} which varies only very slowly in time due to the 'history effect' applied. As a consequence of this 'history effect', physical k_s values are little affected by wetting and drying at nearshore beach locations, with time variations in total k_s being attributable almost entirely to WCI.

Figure 14(a) shows the simulated total bottom k_s at the selected time instant for four different scenarios, namely i) tides alone (no waves), ii) tides + waves without WCI, iii) tides + waves with WCI included and iv) tides + hypothetical waves (wave height on model boundary doubled) with WCI included. Each simulation belongs to Sequence 2d which imposes a cap on the physical k_s beyond ~400 m offshore, as discussed earlier. For tides alone the total k_s near the shore is about 0.17 m, decreasing in the outer part of the transect to ~0.06 m. With waves present, but without WCI, k_s is

enhanced near the shore achieving a maximum value of ~1.0 m in the outer surf zone. When WCI is applied, the total k_s is enhanced further, by a large factor of about 5 at the wave breaking point, decreasing to a factor of about 2 at ~350 m from the shore. When the wave height H_s is doubled (hypothetical case), k_s is increased further at the wave breaking point and then maintains an enhanced value away from the shore.

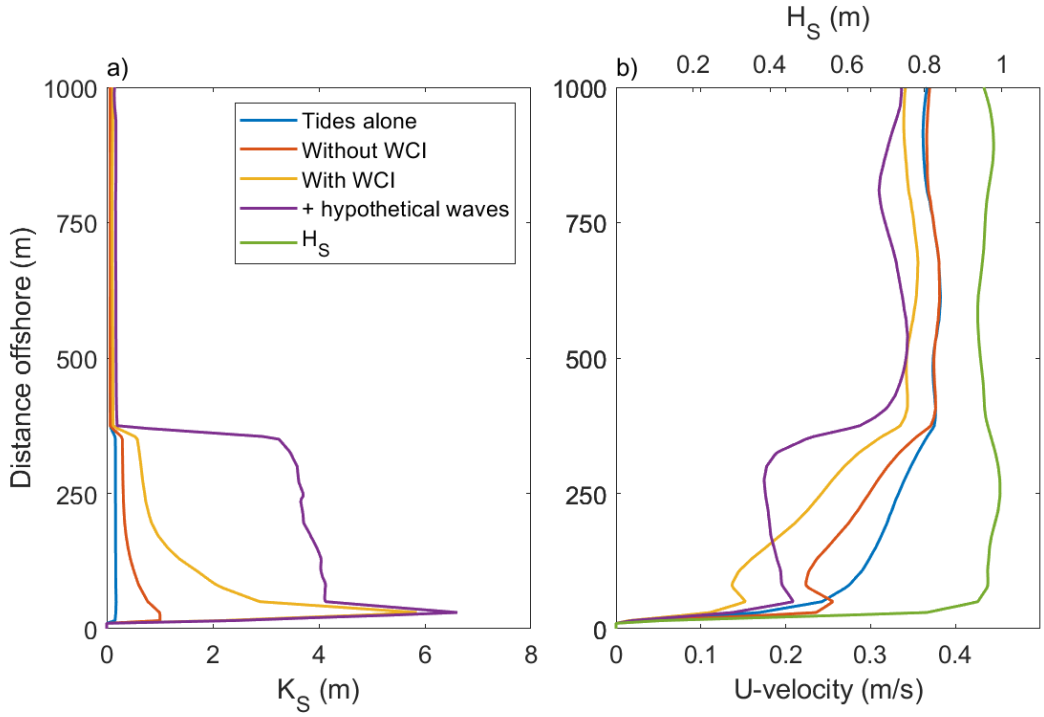

Fig. 14. Illustration of the WCI effect at a NS-transect of length 1 km offshore at Llanddulas promontory (part of Transect 5 in Figure 1). Profiles are drawn with 5 m resolution of (a) the total roughness k_s, and (b) the u-component of velocity (eastward flow is positive), and the significant wave height H_s, for Sequence 2d, during 16 May 2018 at 20:00 hrs. Instantaneous velocity u-profiles are shown for simulations with tides alone, and tides and waves both with and without WCI implemented. Also shown for the case with WCI are results for a hypothetical doubled wave height H_s. The wave breakpoint is at about 50 m offshore for the unadjusted waves.

These k_s enhancements affect the strength of both the tidal currents nearshore, and also the wave-driven currents generated by radiation stresses resulting from wave transformation and breaking. The significant wave height H_s is approximately 1 m across the Llanddulas transect as shown in Figure 14(b) and, with waves incident on the beach at ~140°, the radiation stresses might be expected to generate a longshore current that enhances the tidal current strength towards the east.

But does this happen here? Essentially, with WCI implemented (yellow profile), the competition between i) the radiation stress enhancing the nearshore current and ii) the roughness opposing the current, is won by the latter effect. The current strength just beyond the break point is approximately halved compared with the solution for tides alone (blue profile) and the wave-induced break point jet, located at about 50 m offshore, is not sufficiently strong to reverse the k_s effect. Doubling the wave height (hypothetical case, purple profile) alters the current strength substantially out to ~350 m from shore with the k_s effect remaining predominant. This is highlighted by the solution in which WCI is not implemented (red profile); here the radiation stress effect becomes more pronounced, with the current strength within the surf zone, and out to the break point, increasing somewhat compared with the WCI-case, with a more pronounced jet at the breakpoint. But beyond the breaker line the k_s effect again becomes predominant, with the current strength being reduced compared with the case of tides alone.

As noted previously, the results in Figure 14 represent the most extreme implementation of Soulsby and Clarke's (2005) formulation, through the inclusion of WCI for all components of the physical k_s. In the absence of validation data on site it is not known where within the broad range of outcomes represented by 'With WCI' and 'Without WCI' in Figure 14 the most realistic outcome lies. This requires future experimentation in the nearshore over a range of wave and tidal current conditions, the waves in the present illustration (apart from the hypothetical case) being relatively low ($H_s \sim 1$ m). What is evident is that any degree of WCI applied in the modelling produces a significantly different outcome from the case 'Without WCI', making WCI a necessary consideration and important limiting effect.

5.2 Baroclinic effects

As noted in Section 2, long-term sediment transport in the eastern part of Liverpool Bay is influenced by the density-driven circulation resulting from freshwater riverine runoff primarily from the Dee

and Mersey Estuaries. Polton et al. (2011) found that freshwater influence extends westward along the North Wales coast on springs to 3.5°W and on neaps to 4°W (corresponding to UTM Easting ~466700 and ~433400, respectively), with some seasonal variability (Hopkins and Polton, 2012; Brown et al., 2016). In other words, baroclinicity can affect much, or all, of the region of present interest.

Baroclinic modelling was carried out for the Dee Estuary by Bolaños et al. (2013) who showed that the interactions of offshore (Irish Sea) water and river inflow cause periodic stratification, including within the Welsh and Hilbre Channels, towards the mouth of the estuary. Maximum residual velocities were found to occur at the surface in both tidal channels reaching 20 cm/s, with smaller velocities of up to 10 cm/s occurring near the bottom. These strong residuals weakened along the extension of the Welsh Channel towards the North Wales coast with residual current magnitudes at both surface and bottom being ~5 cm/s, consistent with the present model outcomes. While not strong enough on their own to move sand and gravel, these residuals would be expected to influence sediment transport pathways in the long term.

Polton et al. (2011) demonstrated a clear northward trend in residual surface currents predicted throughout Liverpool Bay, balanced partially by a southward residual flow in the bottom velocities. Palmer and Polton (2011) highlighted 'strain induced periodic stratification (SIPS)', which provides a pumping mechanism that permanently transports freshwater away from the Welsh coastline. They estimated the measured residual flow, well to the north of Constable Bank, to be about 4.0 cm/s to the north at the surface and 2.4 cm/s to the south near the bottom, which promotes upwelling at the Welsh coastline. Brown et al. (2015) studied the effect of baroclinicity on the eastern side of Liverpool Bay and demonstrated that finer sediment particles leaving the Mersey Estuary move northwards, while coarser sediment moves somewhat westwards with baroclinicity limiting the residual sediment circulation out of the estuary. An outcome for the Mersey Estuary consistent with

this was reported in earlier work by Thomas et al. (2002) who compared two- and three-dimensional TELEMAC model solutions. Such a depth-averaged TELEMAC scheme was used by Luo et al. (2015) who argued that the patterns of net sediment transport in Liverpool Bay were similar for two- and three-dimensional simulations.

These baroclinic effects are assessed in relation to the present model outcomes in the section following.

5.3 *Caveats*

The predicted residual velocity and sediment transport patterns for May 2018 present a consistent outcome, both with and without waves present, of a clockwise circulation around the western end of Constable Bank. The same outcome was obtained from a simulation of a somewhat stormier period (October 2014, not presented in this paper) and also from the hypothetical case discussed earlier in which the wave height was doubled. So there seem reasonable grounds to conclude that the clockwise circulation around the end of the bank will be a persistent feature, caused primarily by the interaction of the tidal flows with the bathymetry. However, any model is only as good as its underpinning assumptions, which here include the important assumptions of depth-averaged and barotropic flow, together with procedures and assumptions relating to the seabed composition, the resulting bed roughness, and the sediment transport rate.

The assumptions of depth-averaged and barotropic flow mean that i) baroclinic effects due to freshwater influence and seasonal stratification are excluded and ii) three-dimensional nearshore effects due to waves, such as undertow, are also excluded. Taking these in turn:-

- Seasonal stratification is unlikely to have played a significant role in the shallow waters off the North Wales coast. In contrast, although baroclinic mixing due to freshwater influence (river runoff) does occur here, its dynamical effect is unlikely to have played a significant role

in the shallow waters considered in this paper. It was inferred from the studies cited in Sections 2.2 and 5.2 that baroclinic effects modify the tidal currents in Liverpool Bay and give rise to northward residual currents at the seabed on the order of only 2 to 3 cm/s north of Constable Bank, decreasing to smaller values (probably ~1 cm/s) on its south side and also in the region of the bank itself. These near-bed flows, while being non-negligible, are significantly smaller than the residual current strengths of ~5 cm/s predicted by the present model in the vicinity of Constable Bank. The westward residual on the south side of Constable Bank would most likely be enhanced somewhat by baroclinic effects, while the eastward residual on its north side would be hardly affected. Thus, the conclusions reached about the clockwise residual pattern around Constable Bank still stand when challenged by the additional baroclinic contributions. Further, since maximum (instantaneous tidal) bottom velocities are much larger than the residual velocities, intra-tidal sediment resuspension will not be influenced significantly by residual effects, though the more subtle, long-term, net transport of sediment might be. The modification to residual velocities caused by three-dimensional baroclinic effects means that some minor uncertainty in the present modelling outcomes for net sediment transport must be acknowledged.

- Near to shore the model represents longshore drift in a depth-averaged manner, but three-dimensional processes such as undertow induced by wave transformation and breaking are not represented. In practice, the offshore residual sediment transport referred to earlier might have been enhanced close to shore compared with the predicted transport shown in Figure 11. However, the overall residual flow and transport patterns discussed earlier for the region of Constable Bank will not have been influenced by these localized 3D effects close to shore.

- The 3-grain size mixture applied throughout the model domain is a key assumption and one that could be refined in the light of improved observational evidence. However, it does appear to provide a satisfactory basis for the prediction of the variable k_s made in the present simulations. As for the predicted sediment transport rates, the use of Bijker's transport model excludes some of the more subtle processes known to occur beneath waves and currents (e.g. transport veering when waves are obliquely incident on a current). But Bijker's model has the merit of exhibiting the correct general behaviour for waves combined with currents and can probably be considered to provide a description of sediment transport consistent with the present level of modelling based on an assumed depth-averaged barotropic flow. Although the present model only considers the transport of sand and gravel, the neglect of fine/cohesive sediment transport is well justified for the open sea and coastal areas of primary interest in this paper.

A further caveat concerns the neglect of wind-forcing in the model. As far as wind-driven flow is concerned, this could be of importance in relation to the transport of fine sediment in suspension. But our concern in this paper is only with sediment sizes that are transported near the seabed (as bedload and suspended load). A rough estimate of the wind-driven flow due to wind speeds of, say, 10 and 20 m/s suggest near-surface currents of about 0.13 and 0.26 m/s with these currents being of importance primarily in the upper part of the water column, and being far smaller and insufficient near the bed to move sand-sized sediment on their own. These currents might at most have an episodic influence on residual transport in combination with the tidal and wave effects included in the present modelling, but this would be very small.

6. Conclusions

A 3-way-coupled model of tides, waves and sediment dynamics has been presented for the North Wales coastal area. This represents the addition of waves to the 2-way-coupled scheme developed

by Davies and Robins (2017). The new 3-way-coupling is believed to be appropriate for the relatively shallow coastal waters highlighted, and therefore represents a suitable proof of concept for other coastal geomorphological studies. The model is barotropic and two-dimensional, i.e., depth-averaged. It follows that three-dimensional baroclinic effects associated with seasonal stratification, and fresh-water runoff, are not included. In the near-coastal areas, undertow is not represented and processes like suspended sediment transport are only represented implicitly. However, despite such limitations, the predominant forcing mechanisms, and hydrodynamic and sediment-transport processes occurring off the North Wales coast, are shown to be included satisfactorily in the modelling.

The model has been validated using tide gauge, MBES, and also hydrodynamic data, obtained during May 2018, giving satisfactory results for sea levels, velocities and wave climate. Modelling the bed forms and sediment dynamics is more challenging, but here the simulations also appear to have yielded satisfactory results. Variations in predicted mean grain diameter provide some insight into the transport processes off the North Wales coast. For example, based on the present mixed grain size modelling approach, Constable Bank may be inferred to have a coarsening trend on its south side and a fining trend on its north side, in agreement with observations.

Emphasis has been placed on the prediction of the seabed roughness k_s which has been validated in comparison with observed sub-grid scale bed features using MBES observations carried out with high spatial resolution. Comparisons have been made between the predicted k_s and observed bed form heights determined along nine MBES-transects. With due allowance for the supply of mobile sediment both north and south of Constable Bank, the agreement between model and observations is considered to be quite good. To the knowledge of the authors, no such validation exercise involving waves and tidal currents has been carried out previously in an offshore coastal setting.

Another feature of the modelling is wave-current interaction (WCI) at the seabed, which has the effect of constraining the magnitude of potentially unrealistic wave-generated currents and eddy structures near the coast. WCI is not included as a standard feature of coastal modelling systems, such as TELEMAC, as it should be. However, its present implementation needs further calibration using observational site data.

Residual velocity and sediment transport predictions provide the main modelling outcomes. The 28-day residual velocity results for May 2018 show a tidally-dominated, westward residual on the south side of Constable Bank and an eastward residual of similar magnitude on its north side. The former effect is predicted also for the residual sediment transport, but with a weak westward residual on the north side of the bank. The velocity residuals are shown to originate in the Dee estuary, to follow the shoreline direction, and then split into two westward directed flows, one close to shore and the other directed along the south side of Constable Bank. The residual on the north side of the bank is in the opposite direction giving rise to the clockwise circulation which is predicted to be of magnitude a few centimetres per second. Such a pattern is consistent with the long-term stability of the bank. Close to shore the residual velocity exhibits a westward drift, while the corresponding transport pattern is complicated by the occurrence of local residual transport cells.

Any offshore renewable energy (ORE) intervention, such additional wind farm or tidal impoundment installations off the North Wales coast, would need to be designed taking these flow and sediment transport patterns into account.

Acknowledgements

The authors wish to acknowledge the support of the SEACAMS2 project (Sustainable Expansion of the Applied Coastal and Marine Sectors: R&D Projects SC2_RD_B09, 2016-20, and SC2_RD_B57, 2021-2), the Welsh Government, the Higher Education Funding Council for Wales, the Welsh European Funding Office, and the European Regional Development Fund Convergence Programme. We acknowledge the support of SEEC (Smart Efficient Energy Centre) at Bangor University, part-funded by the European Regional Development Fund (ERDF), administered by the Welsh Government. This project was undertaken in collaboration with NWTE Ltd. (North Wales Tidal Energy Ltd.); in particular, John Reynolds is thanked for contributing his knowledge and insights about the North Wales coastal area. The model simulations were conducted on the Supercomputing-Wales high-performance computing (www.supercomputing.wales) system (a collaboration between Welsh universities and the Welsh Government), supported by Ade Fewings and Aaron Owen. The MBES survey in 2018 was conducted with the involvement of several staff at Bangor University. The work was also supported by the NERC projects SEARCH (NE/V004239/1) and Plastic Vectors (NE/S004548/1).

References

Belderson, R.H., Kenyon, N.H., and Stride A.H., 1977. Sand transport paths. [In Atlas of the Seas Around the British Isles by A. J. Lee and J. W. Ramster.] Fisheries Research Technical Report, Lowestoft, no. 20, sheet 35.

Bijker, E.W., 1992. Mechanics of sediment transport by the combination of waves and current. Proceedings of the 23rd International Conference on Coastal Engineering, American Society of Civil Engineers, Venice, Italy, 147-173.

Bolaños, R., Brown, J.M., Amoudrey, L.O., and Souza, A.J, 2013. Tidal, Riverine, and Wind Influences on the Circulation of a Macrotidal Estuary. Journal of Physical Oceanography, 43, 29-50.

Brown, J.M., Souza, A.J., and Wolf, J., 2010. An 11-year validation of wave-surge modelling in the Irish Sea, using a nested POLCOMS–WAM modelling system. Ocean Modelling, 33, 118–128. https://doi.org/10.1016/j.ocemod.2009.12.006

Brown, J.M., Amoudry, L.O., Souza, A.J., and Rees, J., 2015. Fate and pathways of dredged estuarine sediment spoil in response to variable sediment size and baroclinic coastal circulation. J. Environ. Manage. 149, 209–221. http://refhub.elsevier.com/S1463-5003(16)30117-2/sbref0008

Brown, J., Norman, D., Amoudry, L., and Souza, A., 2016. Impact of operational model nesting approaches and inherent errors for coastal simulations [in special issue: Coastal ocean modelling] Ocean Modelling, 107, 48-63. https://doi.org/10.1016/j.ocemod.2016.10.005

Canadian Hydraulics Centre, 2011. Blue Kenue™: Software tool for hydraulic modellers. National Research Council of Canada. http://www.nrc-cnrc.gc.ca/eng/solutions/advisory/blue_kenue_index.html

Davies, A.G., and Robins, P., 2017. Residual flow, bedforms and sediment transport in a tidal channel modelled with variable bed roughness. Geomorphology, 295, 855-872.

Davies, A.G., Villaret, C., 2002. Prediction of sand transport rates by waves and currents in the coastal zone. Continental Shelf Research, 22 (18-19), 2725-2737.

Davies, A.M., and Jones, J.E., 1996. Sensitivity of tidal bed stress distributions, near-bed currents, overtides, and tidal residuals to frictional effects in the eastern Irish Sea. J. Phys. Oceanography, 26, 2553-2575.

Demmer, J., Neill, S.P., Andres, O., Malham, S.K., Jones, T., and Robins, P., 2022. Larval dispersal from an energetic tidal channel and implications for blue mussel (Mytilus edulis) shellfisheries. Aquaculture International. Published online 16 August 2022. https://doi.org/10.1007/s10499-022-00948-x

Egbert, G.D., Bennett, A.F., and Foreman, M.G., 1994. TOPEX/POSEIDON tides estimated using a global inverse model. Journal of Geophysical Research, 99, 24821-24852.

Halcrow, 2011. North West & North Wales Coastal Group. North West England and North Wales Shoreline Management Plan SMP2. Halcrow Group Ltd, Swindon, UK.

Hervouet, J.-M., 2007. Hydrodynamics of free surface flows, Modelling with the finite-element method. John Wiley and Sons Ltd., West Sussex, England. 340pp.

Hopkins, J., and Polton, J.A., 2012. Scales and structure of frontal adjustment and freshwater export in a region of freshwater influence. Ocean Dynamics, 62:45–62. DOI 10.1007/s10236-011-0475-7

Horrillo-Caraballo, J.M., Yin, Y., Fairley, I., Karunarathna, H., Masters, I., and Reeve, D.E., 2021. A comprehensive study of the tides around the Welsh coastal waters. Estuarine, Coastal and Shelf Science, 254, 107326. https://doi.org/10.1016/j.ecss.2021.107326

Kenyon, N.H., and Cooper, B., 2005. SEA6 - Sand banks, sand transport and offshore wind farms. https://assets.publishing.service.gov.uk/government/uploads/system/uploads/attachment_data/file/197301/SEA6_Sandbanks_Kenyon_Cooper.pdf

Luo, J., Li, M., Sun, Z., and Wang, W., 2015. Impacts of sea level rise on morphodynamics in Liverpool Bay. Proceedings of the Institution of Civil Engineers, Maritime Engineering, 168, 1, 3-19. ISSN 1741-7597 | E-ISSN 1751-7737. https://doi.org/10.1680/maen.14.00012

Marine Institute, 2020. http://www.marine.ie/Home/marine-institute-request-digital-data

Palmer, R.M., and Polton, J.A., 2011. A strain-induced freshwater pump in the Liverpool Bay ROFI. Ocean Dynamics, 61:1905–1915 DOI 10.1007/s10236-011-0430-7

Pawlowicz, R., Beardsley, B., Lentz, S., 2002. Classical tidal harmonic analysis including error estimates in MATLAB using T_TIDE. Computers and Geosciences, 28, 929-937.

Piano, M., Neill, S.P., Lewis, M.J., Robins, P.E., Hashemi, M.R., Davies, A.G., Ward, S.L., and Roberts, M.J., 2017. Tidal stream resource assessment uncertainty due to flow asymmetry and turbine yaw misalignment. Renewable Energy, 114, 1363-1375. https://www.sciencedirect.com/science/article/pii/S0960148117304081

Pingree, R.D., and Griffiths, D.K., 1979. Sand transport paths around the British Isles resulting from M_2 and M_4 interactions. J. mar. biol. Ass. U.K., 59, 497-513.

Plater, A.J., and Grenville, J., 2010. Liverpool Bay: Linking the eastern Irish Sea to the Sefton Coast. In: Worsley, Lymbery, Holden, Newton (Eds.), Sefton's Dynamic Coast, Proceedings of the Conference on Coastal Geomorphology, Biogeography and Management 2008, pp. 28-54.

Polton, J.A., Palmer, R.M., and Howarth, M.J., 2011. Physical and dynamical oceanography of Liverpool Bay. Ocean Dynamics, 61:1421–1439. DOI 10.1007/s10236-011-0431-6

Pope, J.O., Brown, K., Fung, F., Hanlon, H.M., Neal, R., Palin, E.J., and Reid, A., 2021. Investigation of future climate change over the British Isles using weather patterns. Climate Dynamics, https://doi.org/10.1007/s00382-021-06031-0

Pye, K., Blott, S.J., 2010. Geomorphology of the Sefton coast and sand dunes. In: Worsley, Lymbery, Holden, Newton (Eds.), Sefton's Dynamic Coast, Proceedings of the Conference on Coastal Geomorphology, Biogeography and Management 2008, pp. 131-160.

Reynolds International, 2019. Investigation into Constable Bank and the coastal environment off the North Wales coast. Report No: J16374B.318, 6th August 2019.

Robins, P.E., Neill, S.P., Giménez, L., Jenkins, S.R., and Malham, S.K., 2013. Physical and biological controls on larval dispersal and connectivity in a highly energetic shelf sea. Limnology and Oceanography, 58(2), 505-524.

Sly, P.G., 1966. Marine Geological Studies in the Eastern Irish Sea and Adjacent Estuaries. PhD Thesis, University of Liverpool, 2 vols.

Soulsby, R.L., 1997. Dynamics of marine sands. Thomas Telford, London.

Soulsby, R.L., 1990. Tidal-Current Boundary Layers. In The Sea, Volume 9, Part A, Ed. B. Le Méhauté and D.M. Hanes, Wiley Interscience, New York, pp. 523-566.

Soulsby, R.L., Clarke, S., 2005. Bed shear-stresses under combined waves and currents on smooth 344 and rough beds. Report TR 137, HR Wallingford, Wallingford, UK, 22pp.

Soulsby, R.L., Malarkey J., 2005. Net transport rates at Teignmouth, UK. In Van Rijn L.C., Soulsby R.L., Hoekstra P. and Davies A.G. (Eds.), 2005. SANDPIT, Sand Transport and Morphology of Offshore Mining Pits. Aqua Publications, The Netherlands, D1-D8.Stride, A.H., 1963. Current-swept sea floors near the southern half of Great Britain. Quarterly Journal of the Geological Society of London, 119, 175-199.

Thomas, C.G., Spearman, J.R., and Turnbull, M.J., 2002. Historical morphological change in the Mersey Estuary. Continental Shelf Research, 22(11): 1775–1794.

Unsworth, C.A., Austin, M.J., and Van Landeghem, K.J.J., (Accepted 2022). Using a natural laboratory to quantify sediment mobility in the turbulent wake of instrument frames and offshore infrastructure. EGU Annual Convention 2022.

Van Rijn, L.C., 2007. Unified view of sediment transport by currents and waves. 1 Initiation of motion, bed roughness and bed-load transport. Journal of Hydraulic Engineering, 133 (6), 649-667.

Verspecht, F., Rippeth, T.P., Simpson, J.H., Souza, A.J., Burchard, H., and Howarth, M.J., 2009. Residual circulation and stratification in the Liverpool Bay region of freshwater influence. Ocean Dynamics, 59:765–779. DOI 10.1007/s10236-009-0233-2

Villaret, C., Hervouet, J-M., Kopmann, R., Merkel, U., and Davies, A.G., 2013. Morphodynamic modelling using the Telemac finite element system. Computers & Geosciences, 53, 105-113.

Wolf, J., Brown, J.M., and Howarth, M.J., 2011. The wave climate of Liverpool Bay – observations and modelling. Ocean Dynamics, 61, 5, 639-655

Appendix A

Bed roughness (k_s) prediction

Van Rijn's (2007) formulation for the bed roughness contributions arising at sub-grid-scale from small-scale ripples k_{sr}, mega-ripples k_{smr} and dunes k_{sd} depends upon a single parameter, namely the mobility number, defined for combined wave + current flow as:

$$\psi = \{U_c^2 + U_w^2\}/\{(s-1)gd\} \tag{A.1}$$

where U_c is the depth-mean current speed; U_w is the near-bed wave velocity amplitude; $s=\rho_s/\rho$ is the relative sediment density (ρ_s and ρ are the densities of sediment and water respectively); g is the acceleration due to gravity; and $d=d_{50}$ is the median grain diameter.

The local instantaneous roughness contributions were computed in module *sisyphe*, as follows:

i) The roughness of movable small-scale, fully developed, ripples (k_{sr}) is assumed to be equal approximately to the ripple height. Van Rijn's (2007) 'smooth' formula represents k_{sr} over the full ψ-range is as follows:

$$k_{sr} = f_{cs} d_{50}\{85 - 65tanh[0.015(\psi - 150)]\} \tag{A.2}$$

where either the coefficient $f_{cs} = \left(0.25\, d_{gravel}/d_{50}\right)^{1.5}$ with $d_{gravel} = 0.002$ m, or $f_{cs} = 1$ for $d_{50} \leq 0.25 d_{gravel}$. For fine sediment of silt size a separate expression is used:

$$k_{sr} = 20 d_{silt} \text{ for } d_{50} < d_{silt} \text{ where } d_{silt} = 0.000032\, m \tag{A.3}$$

The predicted ripple roughness is maximum in the lower current regime, while the ripples are suppressed at high flow stages, ultimately disappearing in the upper current regime ($\psi \geq 250$).

ii) Mega-ripples (k_{smr}) have a different behaviour, tending first to increase in height, and then decrease, for increasing ψ. The wavelengths of mega-ripples are of the order of, but no greater than, the mean water depth (h), with k_{smr} 'roughly on the order of half the bedform height'. Thus the dominance of small-scale ripples at low wave-current mobility is replaced, in part, by the presence of mega-ripples at higher mobility. Van Rijn's (2007) parameterization of k_{smr} over the full ψ-range is as follows:

$$k_{smr} = 0.00002 f_{fs} h[1 - exp(-0.05\psi)](500 - \psi) \tag{A.4}$$

in which $f_{fs} = d_{50}/1.5 d_{sand}$ where $d_{sand} = 0.000062\, m$, or $f_{fs} = 1$ for $d_{50} \geq 1.5 d_{sand}$. At high flow stages the following expressions are used:

$$\begin{aligned} k_{smr} &= 0.02 \text{ m for } \psi > 550 \text{ and } d_{50} \geq 1.5 d_{sand} \\ k_{smr} &= 200 d_{50} \text{ for } \psi > 550 \text{ and } d_{50} < 1.5 d_{sand} \end{aligned} \tag{A.5}$$

For fine sediment of silt size the mega-ripples are inhibited:

$$k_{smr} = 0 \text{ for } d_{50} < d_{silt} \tag{A.6}$$

iii) Dunes (k_{sd}) have characteristics strongly dependent upon the water depth (h) with wavelengths in the range 3h to 15h and with significant heights, like those of mega-ripples, that first

increase, and then decrease, for increasing mobility. Again, as for mega-ripples, k_{sd} is 'roughly on the order of half the bedform height'. The formula proposed by Van Rijn (2007) for the full ψ-range is:

$$k_{sd} = 0.00008 f_{fs} h[1 - exp(-0.02\psi)](600 - \psi) \quad \text{(A.7)}$$

where the factor f_{fs} is as defined earlier. For high mobility and for fine-grained sediment, the dunes are inhibited:

$$k_{sd} = 0 \quad \text{for} \quad \psi > 600 \quad \text{and for} \quad d_{50} < d_{silt} \quad \text{(A.8)}$$

The above formulation allows maximum k_{sd} values to increase as h increases up to a maximum allowed value of $k_{sd} = 1\ m$. The roughness k_{sd} typically far exceeds the contributions made to the total roughness by k_{smr} and k_{sr}.

iv) The overall roughness due to the sub-grid-scale bed features, is obtained by quadratic summation:

$$k_{s,TOT} = \left[k_{sr}^2 + k_{smr}^2 + k_{sd}^2\right]^{\frac{1}{2}} \quad \text{(A.9)}$$

This quadratic expression, rather than a simple summation, is acknowledged by Van Rijn (2007) to be an intuitive, engineering approach. It is possibly justified for situations where the bedform crest lines are not aligned, such that flows directed, locally and instantaneously, along crests (and troughs) of one or other of the bedform components will not encounter the full roughness of that component but, instead, a sharply reduced value (cf. Soulsby, 1990).

The total roughness is calculated in *sisyphe* at each point of the computational domain, using Equations (A.1) – (A.9), subject to a 'history effect' which is applied to k_{sd}, as explained by Davies and Robins (2017). The total roughness k_s is given by $k_{s,TOT}$ from (A.9), to which is added a granular, skin friction, component k_s' , and k_s is then passed back from *sisyphe* to *telemac2d* (see Figure 2). The sediment transport calculations made in *sisyphe* use only the small-scale ripple roughness k_{sr} (Equations (A.2) & (A.3)) together with k_s'.

Appendix B

Wave-current interaction scheme of Soulsby and Clarke (2005)

The combination of waves and a current in the seabed boundary layer gives rise to increased turbulence and mixing compared with the situation involving the current alone and, hence, to an increased total roughness characterising the outer boundary layer flow. This effect has been represented here using the method of Soulsby and Clarke (2005) for rough beds, which has been implemented in a customized version of the *sisyphe* subroutine *ride.f* :

The essential details of the method are as follows. The bed shear stress due to the current (τ_c) is represented by the quadratic friction law:

$$\tau_c = \rho C_D U^2$$

where U is the depth-averaged velocity, ρ the water density, and C_D the drag coefficient given by the standard expression for a logarithmic velocity profile with physical roughness z_0 (=k_s/30) in water of depth h:

$$C_D = \left(\frac{0.40}{\ln\left(h/z_0\right) - 1} \right)^2$$

The peak bed shear stress due to waves of near-bed excursion amplitude A and period T is represented by:

$$\tau_w = \tfrac{1}{2}\rho f_w U_w^2$$

where U_w (=$2\pi A/T$) is the near-bed wave velocity amplitude, and f_w is the wave friction factor given by Soulsby's (1997) expression:

$$f_w = 1.39\left(A/z_0\right)^{-0.52}$$

The waves and currents interact in the wave boundary layer which has thickness δ. Above this layer the mean bed shear stress (τ_m) is enhanced such that $\tau_m = \rho u_{*m}^2 > \tau_c$ where u_{*m} is the friction velocity for the combined flow in the outer boundary layer.

Inside the wave boundary layer, the 'effective shear stress' ($\tau_e = \rho u_{*e}^2$) is defined by the quadratic sum:

$$\tau_e^2 = \tau_c^2 + \tau_w^2$$

This equation is at the heart of the method. It follows from this assumption that, when the logarithmic mean velocity profiles within and outside the wave boundary layer are matched at height δ, the enhanced wave-current roughness z_{0wc} (= k_{swc}/30) can be expressed in terms of the original, known, roughness z_0 as:

$$\frac{z_{0wc}}{z_0} = \left\{\frac{z_0}{\delta}\right\}^{u_{*m}/u_{*e} - 1}$$

with:

$$u_{*m} = \frac{1}{2a}\left[\left(b^2 + 4aU\right)^{1/2} - b\right]$$

$$a = \frac{1}{\kappa u_{*e}} ln\left(\frac{\delta}{z_0}\right)$$

$$b = \frac{1}{\kappa} ln\left(\frac{h}{e\delta}\right)$$

$$\delta = \frac{0.26 u_{*w} T}{2\pi}$$

and wherein $\tau_w = \rho u_{*w}^2$, $e = exp(1)$ and von Karman's constant κ=0.40.

These are the salient details of the wave-current interaction method, taken from the longer procedure described by Soulsby and Clarke (2005), that are needed for the present implementation of wave-current interaction in *sisyphe*. At each timestep of the model run, known local values of U, U_w, T and h are used to obtain local values of the bed roughness enhancement factor $z_{0wc}/z_0 = k_{swc}/k_s$. The enhanced value of the bed roughness is then fed back into *telemac2d* as indicated in Figure 2.

As discussed in Section 3 and Appendix A, module *sisyphe* predicts the total physical roughness k_s by combining (quadratically) the effects of sand grains, small-scale ripples, mega-ripples and dunes. This local roughness is generally dominated by the dune component k_{sd}, which itself is subject to a 'history effect'. As far as the application of wave-current interaction is concerned the uncertainty that arises is the extent to which some, or all, of these physical roughness components should be included in the calculation of the WCI enhancement factor. The factor is a representation of the additional turbulence caused by WCI and, in practice, this interaction will arise from enhanced mixing above all of small-scale ripples, mega-ripples and dunes. However, the argument underlying the WCI approach rests on a hierarchy of superimposed logarithmic velocity profiles. At present, there is a lack of empirical evidence to calibrate the present implementation of WCI, which has been assumed here to involve all three bed roughness components fully. This implementation is thus a limiting case representing the most severe level of WCI possible through application of Soulsby and Clarke's (2005) method.